Dynamic Average-Value Modeling of Doubly-Fed Induction Generator Wind Energy Conversion Systems

by

Azin Shahab

A Thesis submitted to the Faculty of Graduate Studies of

the University of Manitoba

in partial fulfillment of the requirements of the degree of

MASTER OF SCIENCE

Department of Electrical and Computer Engineering

University of Manitoba

Winnipeg, Manitoba

Copyright © 2013 by Azin Shahab

Abstract

In a Doubly-fed Induction Generator (DFIG) wind energy conversion system, the rotor of a wound rotor induction generator is connected to the grid via a partial scale ac/ac power electronic converter which controls the rotor frequency and speed.

In this research, detailed models of the DFIG wind energy conversion system with Sinusoidal Pulse-Width Modulation (SPWM) scheme and Optimal Pulse-Width Modulation (OPWM) scheme for the power electronic converter are developed in detail in PSCAD/EMTDC. As the computer simulation using the detailed models tends to be computationally extensive, time consuming and even sometimes not practical in terms of speed, two modified approaches (switching-function modeling and average-value modeling) are proposed to reduce the simulation execution time. The results demonstrate that the two proposed approaches reduce the simulation execution time while the simulation results remain close to those obtained using the detailed model simulation.

Acknowledgement

First and foremost, I would like to thank my family for all their support. I would specially like to thank my parents for their endless love and for being there for me whenever I needed them. I deeply appreciate all the life skills they taught me.

I would also like to express my gratitude to my advisor, Dr Shaahin Filizadeh, for his great support and supervision. His deep knowledge and valuable comments helped me a lot during my M. Sc. program.

Finally, I would like to thank all my friends who helped me during my studies.

To my loving parents

Table of Contents

Abstract ii
Acknowledgement iii
Table of Contents v
List of Figures vii
List of Tables ix
Chapter 1 Introduction 1
1.1 Growth of Wind Energy Generation 2
1.2 Features of Wind Energy 3
1.3 Wind Energy Conversion Systems 4
1.4 Problem Definition and Research Objectives 7
1.5 Organization of the Thesis 9
Chapter 2 Wind Energy Conversion Systems 11
2.1 Configurations of Wind Energy Conversion Systems 12
2.1.1 Fixed Speed Configuration 12
2.1.2 Limited Variable Speed Configuration 13
2.1.3 Variable Speed Configuration with a Partial Scale Power Electronic Converter 14
2.1.4 Variable Speed Direct-Drive Concept with a Full-Scale Power Converter 15
2.2 Modeling of a DFIG Wind Energy Generation System 17
2.2.1 Aerodynamic Model 17
2.2.2 Mechanical Model 19
2.2.3 Doubly-fed Induction Generator Model 21
Chapter 3 DFIG Wind Energy Conversion Systems Circuits and Control Schemes 30
3.1 Static Frequency Converter 31
3.1.1 Back-to-Back PWM Converter 32
3.1.2 Back-to-Back PWM Converter Modulation Schemes 33
3.1.2.1 Sinusoidal Pulse Width Modulation (SPWM) 34
3.1.2.2 Optimal Pulse Width Modulation (OPWM) 35
3.2 DFIG Wind Energy Conversion Systems Control Schemes 36
3.2.1 Back-to-Back PWM Converter Control Schemes 37
3.2.2 Mechanical Control 47
3.2.2.1 Wind Turbine Operating Regions 47
3.2.2.2 Wind Speed Measurement Method 50

Chapter 4 Back-to-Back PWM Converter 52

4.1 Switching- Function Model 53

4.2 Dynamic Average-Value Modeling.....60
4.2.1 Dynamic Average-Value Modeling Technique in DFIG Simulation..... 61
4.2.1.1 Concept of Average-Value Modeling..... 61
4.2.1.2 Application of Average-Value Modeling in DFIG Simulation 64
4.3 Reduced Intensity Simulation of a Wind Farm Connected to the Power System Network…… 70

Chapter 5 Conclusions, Contributions, and Suggestions for Future Work……...75

5.1 Conclusions and Contributions.....75
5.2 Suggestions for Future Work.....77

References..... 79

List of Figures

Fig. 1.1. World total installed wind capacity (MW) 2
Fig. 1.2. Total installed wind capacity in Canada (MW) 3
Fig. 1.3. General block diagram of a wind energy conversion system 5
Fig. 1.4. Scheme of a system with DFIG concept 6
Fig. 1.5. Back-to-Back PWM converter 7

Fig. 2.1. Fixed speed configuration with SCIG system (Adopted from [7]) 13
Fig 2. 2. Limited variable speed configuration with WRIG system (Adopted from [7]) . 14
Fig. 2.3. Variable speed configuration with DFIG system (Adopted from [7]) 15
Fig. 2.4. Direct-drive electrically excited synchronous generator (EESG) configuration (Adopted from [7]) 16
Fig. 2.5. Direct-drive permanent magnet synchronous generator (PMSG) configuration (Adopted from [7]) 16
Fig 2. 6. Performance coefficient, C_p, as a function of tip speed ratio λ, with pitch angle θ as a parameter 19
Fig. 2.7. Mechanical model of wind energy conversion system 20
Fig 2. 8. Wound rotor induction generator 22
Fig. 2.9. qd0 reference frame 25

Fig. 3.1. Back-to-Back PWM converter 33
Fig. 3. 2. SPWM scheme (Adopted from [21]) 34
Fig. 3. 3. OPWM scheme (Adopted from [21]) 36
Fig. 3.4. DFIG wind energy conversion system 37
Fig. 3.5. Rotor-side converter control scheme 40
Fig. 3. 6. Grid-side converter model 41
Fig. 3.7. Grid-side converter control block diagram 43
Fig. 3. 8. DFIG wind energy conversion system with SPWM scheme 45
Fig. 3. 9. DFIG wind energy conversion system with OPWM scheme 46
Fig. 3. 10. Wind turbine characteristics with $V_{w1}>V_{w2}>V_{w3}>V_{w4}>V_{w5}$ 48
Fig. 3.11. Wind turbine operating regions 49

Fig. 4. 1. The rectifier detailed model 54
Fig. 4.2. The rectifier equivalent switching-function model 55
Fig. 4.3. Rectifier switching- function model in PSCAD/EMTDC 56
Fig. 4.4. Calculation of voltage sources input values in rectifier switching-function model in PSCAD/EMTDC 56
Fig.4.5. Calculation of current sources input values in rectifier switching-function model in PSCAD/EMTDC 57

Fig. 4. 6. SPWM modulation, switching-function and detailed model results 58
Fig. 4. 7. OPWM modulation, switching-function and detailed model results 59
Fig. 4. 8. SPWM scheme and average-value output 62
Fig. 4.9. Rectifier average-value voltages and currents in the dq reference frame..... 65
Fig. 4. 10. The rectifier model 66
Fig. 4. 11. The rectifier average-value model 66
Fig. 4.12. Average-value modeling with rectifier as an algebraic block (Adopted from [26])..... 67
Fig. 4.13. Equivalent average-value model for the rectifier in PSCAD/EMTDC 68
Fig. 4. 14. EMT detailed SPWM and average-value models results 69
Fig. 4. 15. Wind farm (WF) connected to the 12 bus system 71

List of Tables

Table 3.1. DFIG rating specifications used in simulation 44
Table 4.1. Simulation execution time for switching-function and EMT detailed models 60
Table 4.2. Simulation execution time for average-value model and EMT detailed model 68
Table 4.3. Rating data of the test power system 72
Table 4.4. Simulation execution time for the wind farm connected to the test power system 73

Chapter 1

Introduction

Today the world is faced with environmental issues such as air pollution and greenhouse gas effects, which threaten both human health and ecosystem. Fossil fuels as a conventional source of energy have a major role in increasing air pollution and destroying air quality. Emitted gases from combustion of fossil fuels in power plants result in climate change, acid rain, and smog, and increase the level of air toxics such as mercury and heavy metals [1], [2]. Also the reserves of fossil fuels are limited. As a result, production of energy from renewable sources such as wind is of great interest. In fact, for every 1 kWh of electrical energy generated by wind, the emission of carbon dioxide (the leading greenhouse gas) is reduced by 1kg, and the operation of a wind turbine weighing 50 tons saves burning of 500 tons of coal annually [2].

1.1 Growth of Wind Energy Generation

Wind as a renewable source of energy, which offers energy production at reduced pollution level, is attracting increasing global attention. Figure 1.1 illustrates the global total installed wind power capacity during the past 10 years [3]. According to the figure, on average, the global wind power capacity has doubled every 3 years over the past decade, and has crossed 200 GW as of the present time. The Global Wind Energy Council (GWEC) estimates that this trend will continue during the next decade as well, and the total wind power installations will reach up to 709 GW by 2020, contributing 8.2% of the world's electricity demand [1, 2, 3].

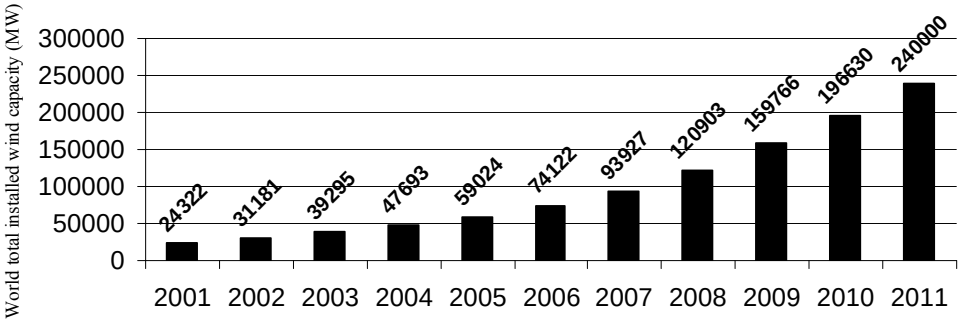

Fig. 1.1. World total installed wind capacity (MW)

In Canada, electricity generated from wind energy powers 1.2 million homes and businesses. Fig 1.2 illustrates the total installed wind capacity in Canada over the past decade [4].

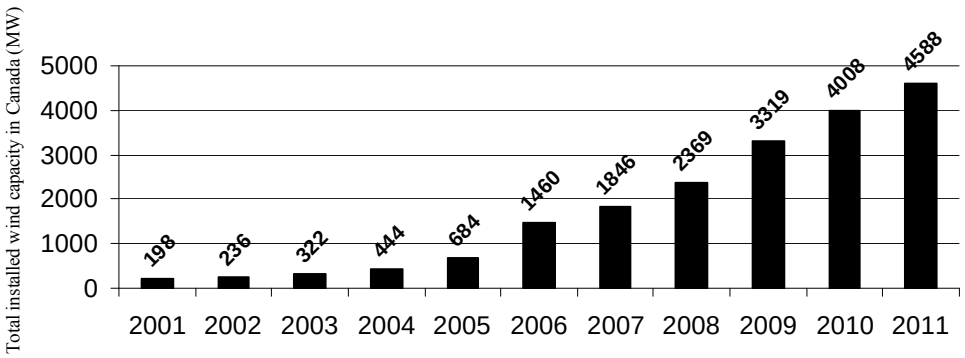

Fig. 1.2. Total installed wind capacity in Canada (MW)

It can be seen from Figures 1.1 and 1.2 that there is a steady growth in wind energy installation in Canada and around the world.

1.2 Features of Wind Energy

Wind energy systems are powered by the naturally blowing wind; therefore they can be considered as a clean source of energy. There are several advantages offered by wind energy, including [5, 6]:

- Unlike conventional power plants that rely on combustion of fossil fuels and cause air pollution, wind energy does not produce atmospheric emissions that cause acid rain or greenhouse gases.
- Unlike fossil fuels, wind energy is available in many regions, and is not limited to a few countries.
- Wind energy generation can benefit the economy in rural areas, as wind turbines could be easily built on farms where most of the best wind sites are found. The

wind turbines only occupy a small fraction on a farm, for which the wind power plant owners make rent payments to the farmer.

However, there are a number of challenging issues about wind energy conversion systems and they have been subject of public arguments recently; these include [5], [6]:

- Wind energy is not continuously available at the same rate
- Wind energy can be costly, specially due to the fact that construction of wind farms is expensive
- Wind turbine blades are sources of noise emission.
- The oscillating shadow of rotating wind turbine blades can be a source of optical disturbance for residents and minimum distances are required.
- Wind energy conversion systems have a negative impact on the landscape phenotype. This issue is of more challenging in the areas where tourism is of economical importance.
- Although nature reserves and national parks are typically not used for installing wind energy conversion systems, wind turbines are dangerous for flying birds.

1.3 Wind Energy Conversion Systems

Wind energy conversion systems typically consist of a wind turbine, an electric generator and possibly the corresponding power electronic converters and control systems, as illustrated in Fig. 1.3.

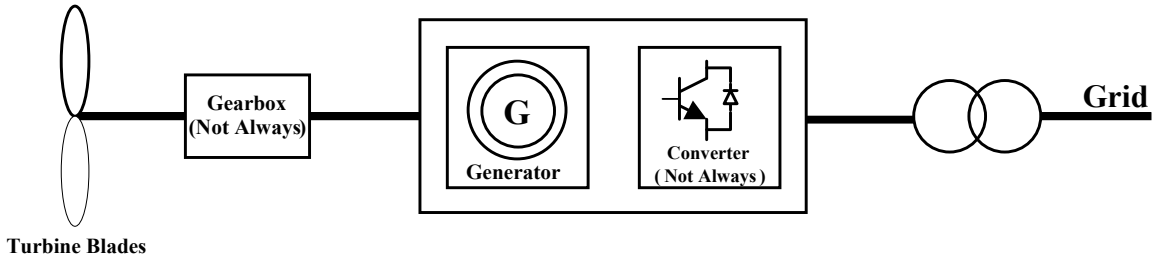

Fig. 1.3. General block diagram of a wind energy conversion system

There are different configurations for wind energy conversion systems, and they can be categorized into four main concepts in terms of the rotation speed and the rating of power electronic converter relative to the generator capacity. These include:

- Fixed speed concept
- Limited variable speed concept
- Variable speed concept with a partial scale power electronic converter
- Variable speed direct-drive concept with a full-scale power converter

These schemes will be described in detail later in Chapter 2.

The 3rd scheme, i.e. variable speed concept with a partial scale power electronic converter (also known as doubly-fed induction generator or DFIG concept), is the scheme of interest in this research. This scheme is the most popular configuration used in wind farms due to its two main advantages that make this concept attractive from an economic point of view. These are:

- Depending on the size of the frequency converter, this concept supports a wider speed range operation, typically 30% around the synchronous speed.

- The rating of the power electronic converter is only 25–30% of the generator capacity.

A DFIG wind energy conversion system using a wound rotor induction generator (WRIG) and a partial-scale power converter on the rotor circuit is illustrated in Fig. 1.4.

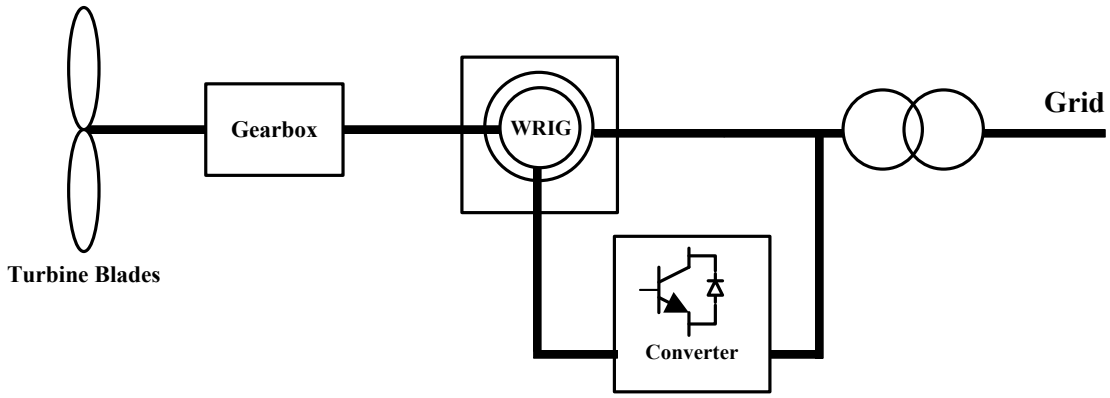

Fig. 1.4. Scheme of a system with DFIG concept

In this scheme, the stator is directly connected to the grid, and the rotor is connected through a power electronic converter. The power electronic converter controls the rotor frequency and thus the rotor speed. As mentioned previously, the rating of the power electronic converter is only about 25–30% of the generator capacity, which makes this concept popular from an economic point of view [7].

At present, excitation converters used in DFIG wind energy conversion systems include cycloconverters, back-to-back pulse-width modulation (PWM) converters and matrix converters, among which the back-to-back PWM converter is the most commonly used configuration [8].

A back-to-back PWM converter (see Fig. 1.5) consists of two pulse-width modulated voltage source converters connected to each other via a dc link. One converter operates in the rectifier mode while the other one performs as an inverter.

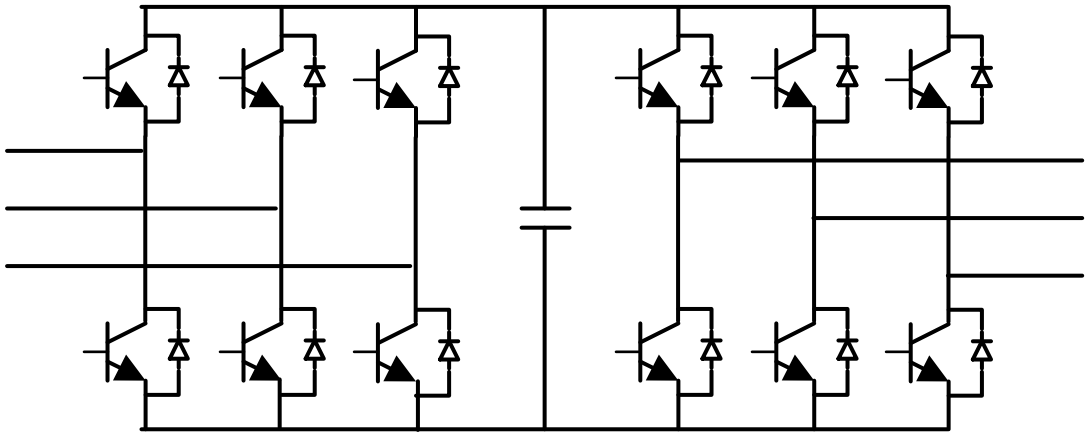

Fig. 1.5. Back-to-back PWM converter

1.4 Problem Definition and Research Objectives

Simulation is an essential step in design and analysis of wind energy conversion systems, as it enables the engineer to select appropriate components and control schemes. Also it offers the engineer an opportunity to analyze and evaluate the wind energy conversion system performance and to verify that it meets the required specifications to be connected to the grid [10].

Ideally, a detailed simulation model for the wind energy conversion system should provide a strong tool for studies. However, in practice there are a number of limitations

including simulation speed in using detailed models for wind energy conversion system studies.

Simulation speed is often a major consideration in design and analysis of wind energy conversion systems. For instance, in order to identify key parameters in the design of a wind farm, simulations need to be repeated several times. Also to study the operation of the wind farm connected to the grid, a detailed simulation may consume a long time. There are several wind turbines, and therefore several power electronic converters in a wind farm. While traditional detailed-model simulation provides accurate results, it requires extensive computations over long time periods. This is mainly due to the existence of power electronic switches, since high switching rates slow down the simulation [9]. In fact, the simulation speed may be so slow that the simulation cannot be completed within the required time. Therefore, it is necessary to simplify detailed models of the wind energy generation system and consequently increase the simulation speed.

The objective of this research is to apply fast simulating techniques as alternatives to the detailed model and compare the results of detailed simulation and fast simulation of wind energy conversion systems in terms of accuracy and run-time. Two fast simulating techniques, namely average-value modeling and switching-function modeling are proposed in this research. For this purpose, first the detailed model of a DFIG wind power generation system is developed in the PSCAD/EMTDC electromagnetic transient simulation program. Two conventional modulation schemes for the power electronic converter, Sinusoidal Pulse Width Modulation (SPWM) and Optimized Pulse-Width Modulation (OPWM), are separately applied to the PSCAD/EMTDC model. These

detailed models are used as benchmarks for the next simulations in which fast simulating techniques are used.

The detailed SPWM and OPWM models are simplified using two approaches. In these approaches, average-value modeling technique and switching-function technique are applied to the both types of the detailed DFIG wind energy conversion system models, respectively. The simplified models are verified in terms of accuracy and the simulation speeds. The results are compared to those obtained from the detailed models.

As a further step, the detailed and simplified models are used in simulation of a wind farm consisting of twenty identical DFIG wind energy conversion systems. This wind farm is studied in connection to a power system. The corresponding simulation run times using the simplified models and detailed models are recorded and compared.

1.5 Organization of the Thesis

In this thesis, the detailed models of DFIG wind energy conversion systems are developed, the fast simulating concepts are presented as alternatives to the detailed models, and the results obtained using the simplified and detailed models simulation are compared. The organization of the rest of the thesis is as follows.

Chapter 2 provides a background on wind energy conversion systems among which the DFIG systems are the focus of the research described in this thesis. The concepts of aerodynamical, mechanical and generator modeling of the DFIG wind energy conversion system are described.

In Chapter 3, the power electronic converters used in DFIG wind energy conversion systems are discussed. The main modulating schemes, i.e. SPWM and OPWM are described, and the corresponding control schemes for the power electronic converter along with the mechanical control of the wind energy conversion system are presented. Also the simulation results for the detailed models of the DFIG wind energy conversion system are illustrated.

In Chapter 4, two fast simulating techniques are described. Application of these techniques on DFIG wind energy conversion systems in PSCAD/EMTDC is presented and the simulation results are compared with those obtained from using detailed models. Also, the detailed and simplified models of a wind farm which is connected to a power system are examined, and the execution times are recorded and compared.

In Chapter 5 the conclusions and the thesis contributions are presented and the possible future studies on this subject are discussed.

Chapter 2

Wind Energy Conversion Systems

Wind energy conversion system (WECS) can be used to capture the energy contained in wind and convert it to electrical energy. What distinguishes wind from other conventional sources of energy, such as coal and gas, is its intermittency and variability. A wind turbine can be used to act as a prime mover for an electric generator. However, due to the variations in wind speed, a gearbox can be used to adjust the rotor shaft speed. The gearboxes used are step-up ones that increase the speed at their output, which is connected to the shaft of the generator. Due to the limitations of using a gearbox (which are described in section 2.1.1) direct use of the converted electric energy for integration into an ac network can cause negative impacts on the ac network. To disallow wind speed variations to impact the receiving electric network, an intermediate power

-electronic system can be used. Therefore, wind energy conversion systems generally can consist of a wind turbine, an electric generator, power electronic converters and/or gearboxes and corresponding control systems.

2.1 Configurations of Wind Energy Conversion Systems

With regards to their rotation speed, wind energy conversion systems can be classified into three main categories: (i) fixed speed configuration, (ii) limited variable speed configuration, and (iii) variable speed configuration. Additionally, variable speed wind energy conversion systems can be further classified into wind generator systems with a partial scale or a full-scale power electronic converter, based on the rating of the power electric converter relative to the generator capacity [7].

In the following sections, an overview of these general categories of wind energy conversion systems will be presented.

2.1.1 Fixed Speed Configuration

The fixed speed wind energy conversion systems use a squirrel cage induction generator (SCIG). The rotor shaft is connected to the turbine through a multi-stage gearbox. The multi-stage gearbox enables the generator to operate in a narrow range around the synchronous speed. The fixed speed wind energy conversion system is illustrated in Fig. 2.1 [7], [8].

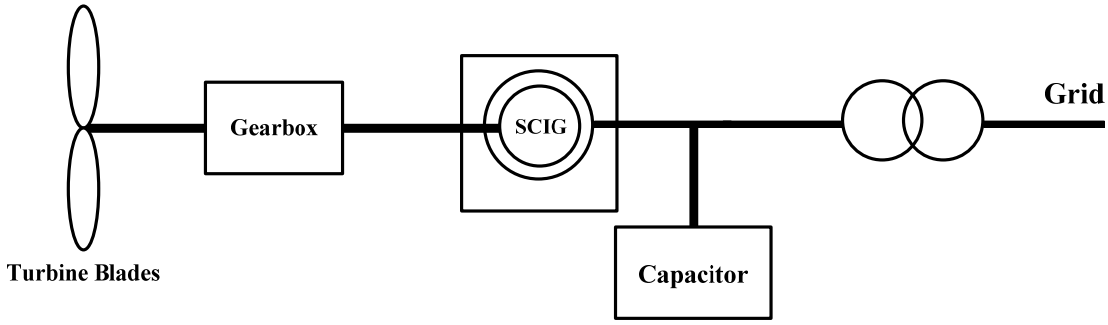

Fig. 2.1. Fixed speed configuration with SCIG system (Adopted from [7])

The main advantages of this concept are its robust and easy configuration. However, in this configuration the speed can be varied only in a narrow range and a multi-stage gear box is bulky and relatively expensive. These major disadvantages limit the application of this type of wind energy conversion system [7].

2.1.2 Limited Variable Speed Configuration

This wind energy conversion system configuration uses a wound rotor induction generator (WRIG) with variable rotor resistance, which is provided by means of a power electronic converter and the pitch control method, as illustrated in Fig 2. 2.

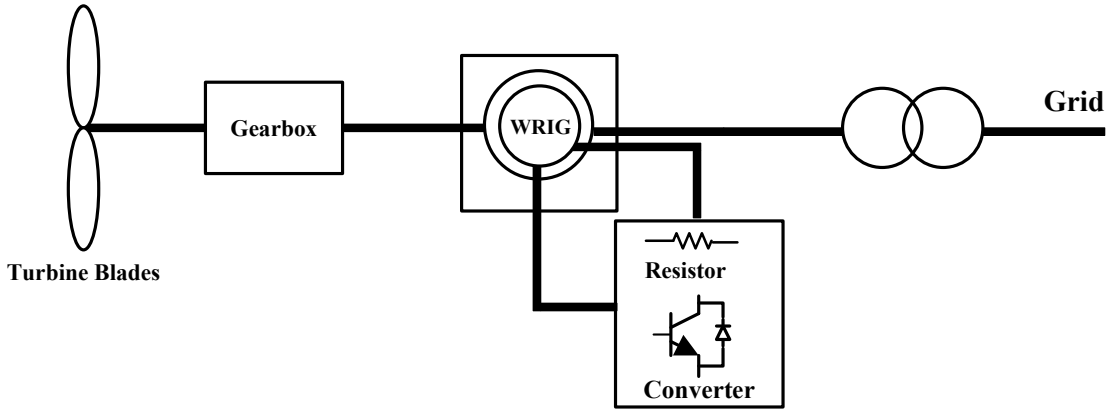

Fig 2. 2. Limited variable speed configuration with WRIG system (Adopted from [7])

In this scheme, the power extracted from the rotor is dissipated in the form of thermal energy in the resistor. The rating of the external resistor depends on the amount of the dissipated power. As the speed variation range increases, the dissipated power will be larger. Therefore, in this scheme the speed variation range is usually limited to 10% above the synchronous speed to limit the losses and the rating of the external resistor [7].

2.1.3 Variable Speed Configuration with a Partial Scale Power Electronic Converter

In this scheme, the rotor of a WRIG is connected to the grid via a partial scale power electronic converter, which controls the rotor frequency and speed. This configuration is referred to as the doubly-fed induction generator, as both the stator and rotor are being fed from the grid.

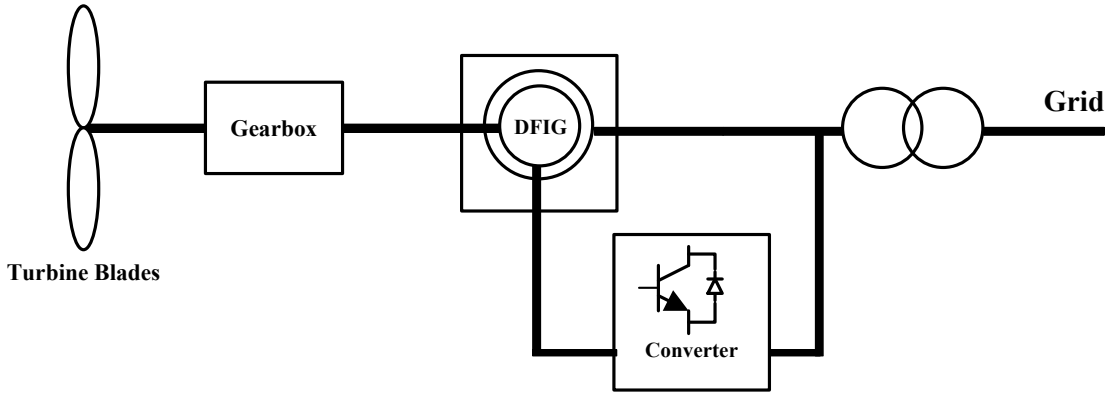

Fig. 2.3. Variable speed configuration with DFIG system (Adopted from [7])

Depending on the size of the frequency converter, this concept supports a wider speed range operation, typically 30% around the synchronous speed. Moreover, the rating of the power electronic converter is only 25–30% of the generator capacity. These two main advantages make this configuration appealing from an economic point of view.

The most commonly used power electronic converter in this scheme is back-to-back PWM converter. The back-to-back PWM converter will be described in detail in Chapter 3.

2.1.4 Variable Speed Direct-Drive Concept with a Full-Scale Power Converter

In this configuration the stator of a direct-drive induction generator is connected to the grid through a power electronic converter. Most frequently, a synchronous generator, either with external electrical excitation (EESG) or permanent magnets (PMSG) are used in this scheme, as illustrated in Fig. 2.4 and Fig 2.5.

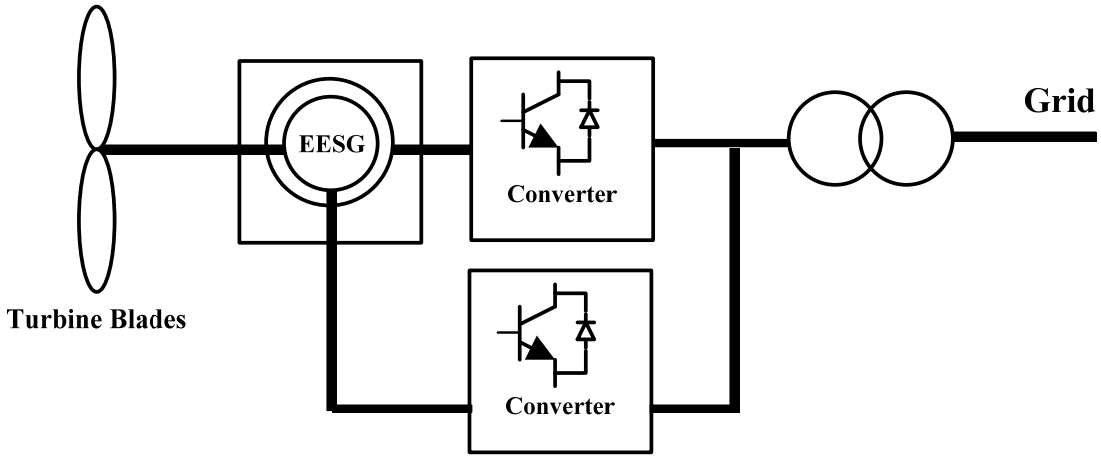

Fig. 2.4. Direct-drive electrically excited synchronous generator (EESG) configuration (Adopted from [7])

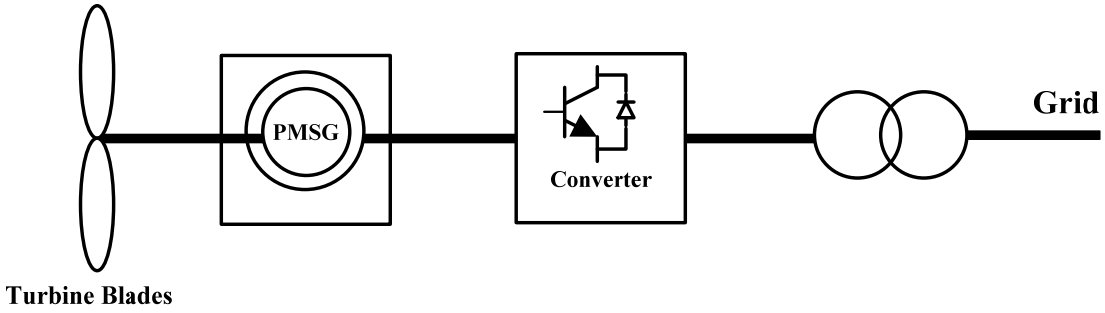

Fig. 2.5. Direct-drive permanent magnet synchronous generator (PMSG) configuration (Adopted from [7])

The direct-drive generator rotates at a lower speed compared to geared-drive wind turbines, as the generator rotor is directly connected on the hub of the turbine rotor. To

deliver a certain power, the lower speed makes it necessary to produce a higher torque which results in a larger size of the generator [7].

Currently doubly-fed induction generators (DFIGs) comprise the most popular category of wind energy conversion systems. As such the attention of the rest of the thesis will be on this category. In the following section, a mathematical model for a DIFG will be developed. This model will later be implemented in an electromagnetic transient simulator for computer simulation-based studies.

2.2 Modeling of a DFIG Wind Energy Generation System

A comprehensive model of a DFIG wind energy conversion system must be taken into consideration. The aerodynamic model, mechanical model and the doubly-fed induction generator model are presented in the following sections. Modeling of corresponding power electronic converter is described in detail in Chapter 3.

2.2.1 Aerodynamic Model

Wind turbines extract mechanical power from wind streams, and transmit it to the electrical generator. An aerodynamic model is used to compute the output extracted mechanical power from wind energy as follows [9, 10].

$$P_{mech} = \frac{\rho}{2} A_r . v_w^3 . C_p(\lambda, \theta) \tag{2.1}$$

where

P_{mech} = mechanical power extracted from the wind [W]

ρ = air density [kg/m^3]

A_r = area covered by the rotor [m^2]

v_ω = wind speed [m/s]

C_p = performance coefficient (or power coefficient)

λ = tip speed ratio

θ = rotor blade pitch angle [deg]

Tip speed ratio, λ, is defined as follows.

$$\lambda = \frac{\omega_T . R}{v_w} \tag{2.2}$$

where

ω_T = angular speed of the turbine shaft [rad/s]

R = wind turbine radius [m]

The mechanical torque extracted from turbine rotor, T, is given by

$$T = \frac{\rho}{2\omega_T} A_r v_w^3 C_p(\lambda, \theta) \tag{2.3}$$

There are different alternatives to model variation of the power coefficient, C_p, vs. rotor blade pitch angle and the tip speed ratio. These include lookup tables or fitted equations [11]. There are several fitted equations for the power coefficient in literature such as the one given below, which is generally descriptive for different types of wind turbines [12, 14].

$$C_p(\lambda,\theta) = 0.22(\frac{116}{\lambda_i} - 0.4\theta - 5)e^{\frac{-12.5}{\lambda_i}} \tag{2.4}$$

where

$$\frac{1}{\lambda_i} = \frac{1}{\lambda + 0.08\theta} - \frac{0.035}{\theta^3 + 1} \tag{2.5}$$

Fig 2. 6 represents the characteristics of $C_p(\lambda,\theta)$ vs. λ for different values of θ.

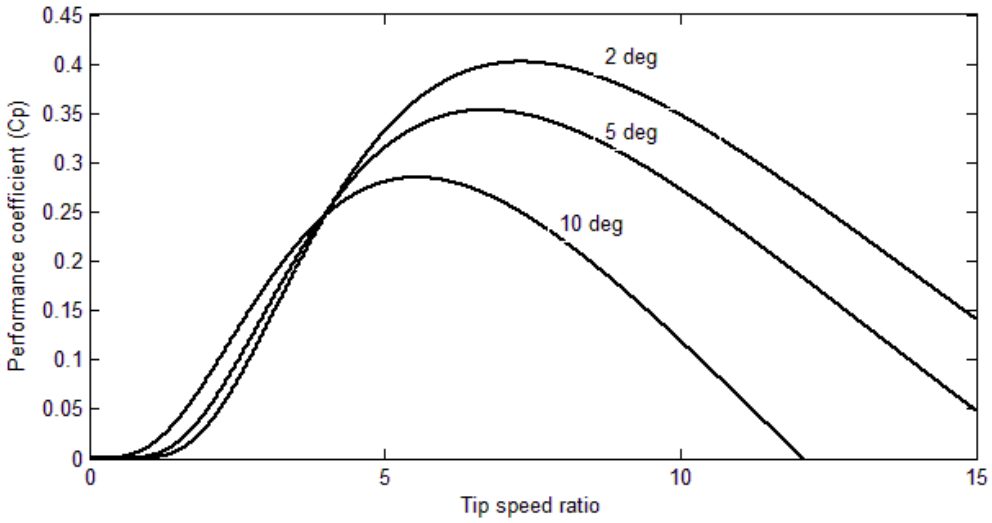

Fig 2. 6. Performance coefficient, C_p, as a function of tip speed ratio λ, with pitch angle θ as a parameter

2.2.2 Mechanical Model

A wind turbine drive train is fundamentally comprised of three masses corresponding to a large mass for the wind turbine rotor, a mass for the gearbox and a

mass for the generator. The moments of inertia of the shafts and gearbox can be neglected because they are small compared to the moments of inertia of the wind turbine and the generator. Therefore, the mechanical model is essentially a two-mass model, as demonstrated in Fig. 2.7. [13, 19]:

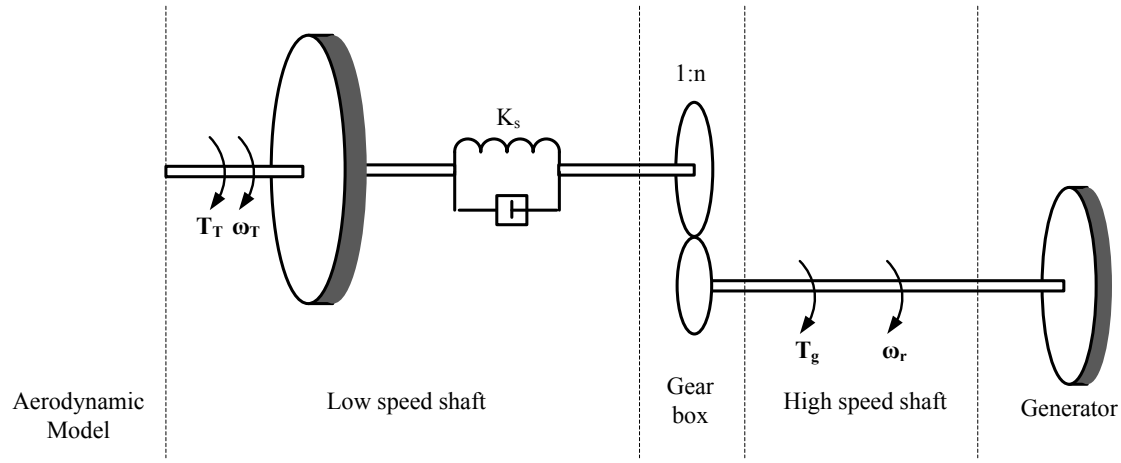

Fig. 2.7. Mechanical model of wind energy conversion system

A two-mass representation has been chosen here, which is described by the following [16]:

$$\frac{d\omega_T}{dt} = \frac{T_T - K_s\gamma}{2H_T} \tag{2.6}$$

$$\frac{d\frac{\omega_r}{n}}{dt} = \frac{K_s\gamma - nT_g}{2H_g} \tag{2.7}$$

$$\frac{d\gamma}{dt} = 2\pi f(\omega_T - \frac{\omega_r}{n}) \tag{2.8}$$

where

f = the nominal grid frequency [Hz]

T_g = generator electromechanical torque [N.m]

T_T = wind turbine torque [N.m}

γ = angular displacement between the two ends of the shafts [rad]

ω_T = wind turbine angular speed [rad/s]

ω_r = rotor angular speed [rad/s]

K_s = shaft stiffness [rad]

H_g = generator inertia constant [kg.m^2]

H_T = wind turbine inertia constant [kg.m^2]

2.2.3 Doubly-fed Induction Generator Model

In this section, a dynamic model for the DFIG is presented. A three-phase induction machine consists of a stator and a rotor. Each phase of the stator and rotor windings has a distributed coil structure. The balanced three-phase ac voltages in the stator induce current in the rotor windings by induction. A schematic of the cross section of an induction machine is illustrated in Fig 2. 8. Although the coils are distributed, they are represented as concentric for simplicity. Letters *r* and *s* denote rotor and stator coils, respectively. Letters *a*, *b* and *c* denote three phase coils.

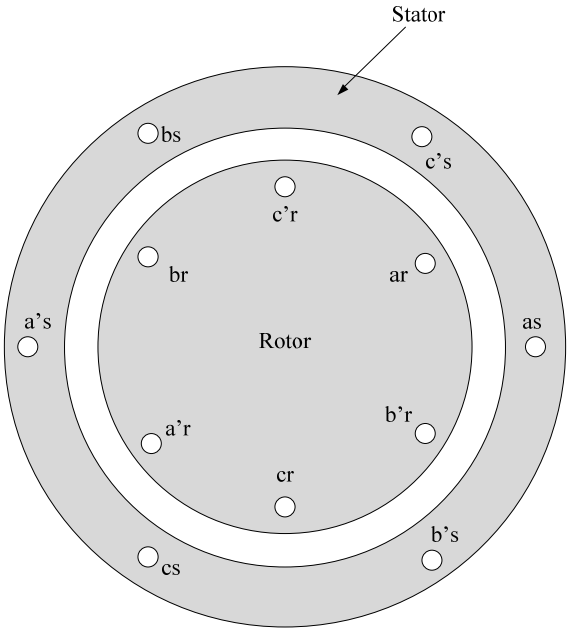

Fig 2. 8. Wound rotor induction generator

The stator current establishes a sinusoidal magnetic flux density wave in the air gap, which rotates at synchronous speed. The corresponding synchronous speed can be calculated by the equation below.

$$\omega_s = \frac{2}{P}\omega_e \tag{2.9}$$

where

ω_s= the synchronous mechanical speed (Mech. rad/sec)

ω_e= stator angular frequency (Elec. rad/sec)

P = the number of poles.

If the mechanical shaft speed of the machine is defined as ω_r (in mech. rad/sec), at any synchronous speed ω_s, the speed difference ω_s - ω_r creates slip (s). The slip is defined as follows:

$$s = \frac{\omega_s - \omega_r}{\omega_s} \tag{2.10}$$

In an induction generator, at steady-state operating point, ω_r is slightly higher than ω_s, while in an induction motor ω_r is slightly lower than ω_s.

The stator and rotor voltages of a DFIG can be represented as a function of the corresponding stator and rotor flux linkages and input currents as follows:

$$\begin{bmatrix} v_{as} \\ v_{bs} \\ v_{cs} \end{bmatrix} = R_s \begin{bmatrix} i_{as} \\ i_{bs} \\ i_{cs} \end{bmatrix} + \frac{d}{dt} \begin{bmatrix} \lambda_{as} \\ \lambda_{bs} \\ \lambda_{cs} \end{bmatrix} \tag{2.11}$$

$$\begin{bmatrix} v_{ar} \\ v_{br} \\ v_{cr} \end{bmatrix} = R_r \begin{bmatrix} i_{ar} \\ i_{br} \\ i_{cr} \end{bmatrix} + \frac{d}{dt} \begin{bmatrix} \lambda_{ar} \\ \lambda_{br} \\ \lambda_{cr} \end{bmatrix} \tag{2.12}$$

R_s and R_r represent the stator and rotor winding resistances, which are assumed to be equal for all phase windings. The subscripts r and s denote rotor and stator quantities, respectively. The subscripts a, b and c stand for phases a, b and c quantities.

The flux linkages of rotor and stator relate to the currents by the inductances:

$$\begin{bmatrix} \lambda_{as} \\ \lambda_{bs} \\ \lambda_{cs} \end{bmatrix} = \mathbf{L_s} \begin{bmatrix} i_{as} \\ i_{bs} \\ i_{cs} \end{bmatrix} + \mathbf{L_m} \begin{bmatrix} i_{ar} \\ i_{br} \\ i_{cr} \end{bmatrix} \tag{2.13}$$

$$\begin{bmatrix} \lambda_{ar} \\ \lambda_{br} \\ \lambda_{cr} \end{bmatrix} = \mathbf{L_m^T} \begin{bmatrix} i_{as} \\ i_{bs} \\ i_{cs} \end{bmatrix} + \mathbf{L_r} \begin{bmatrix} i_{ar} \\ i_{br} \\ i_{cr} \end{bmatrix} \tag{2.14}$$

The inductance matrices $\mathbf{L_s}$, $\mathbf{L_r}$ and $\mathbf{L_m}$ are defined as:

$$\mathbf{L_s} = \begin{bmatrix} L_{ls} + L_m & \frac{-1}{2} L_m & \frac{-1}{2} L_m \\ \frac{-1}{2} L_m & L_{ls} + L_m & \frac{-1}{2} L_m \\ \frac{-1}{2} L_m & \frac{-1}{2} L_m & L_{ls} + L_m \end{bmatrix} \tag{2.15}$$

$$\mathbf{L_r} = \begin{bmatrix} L_{lr} + L_m & \frac{-1}{2} L_m & \frac{-1}{2} L_m \\ \frac{-1}{2} L_m & L_{lr} + L_m & \frac{-1}{2} L_m \\ \frac{-1}{2} L_m & \frac{-1}{2} L_m & L_{lr} + L_m \end{bmatrix} \tag{2.16}$$

$$\mathbf{L_m} = L_m \begin{bmatrix} \cos(\theta_r) & \cos(\theta_r + \frac{2\pi}{3}) & \cos(\theta_r - \frac{2\pi}{3}) \\ \cos(\theta_r - \frac{2\pi}{3}) & \cos(\theta_r) & \cos(\theta_r + \frac{2\pi}{3}) \\ \cos(\theta_r + \frac{2\pi}{3}) & \cos(\theta_r - \frac{2\pi}{3}) & \cos(\theta_r) \end{bmatrix} \tag{2.17}$$

where

L_{ls} = stator leakage inductance

L_{lr} = rotor leakage inductance

L_m = the maximum amplitude of the mutual inductance between the stator and the rotor

θ_r = The rotor electric angular displacement (in elec. rad/sec) regarding to the stator, which can be calculated as follows:

$$\theta_r(t) = \int_0^t \omega_r dt' + \theta_r(0) \tag{2.18}$$

According to equations (2.17) and (2.18), the mutual inductance matrix $\mathbf{L_m}$ depends on time. In order to eliminate this time dependency, it is convenient to switch to a more suitable reference frame by using the *dq0*- transformation.

The *dq0*-reference frame is a rotating reference frame rotating at a speed of choice. In this thesis, the *dq0*-reference frame rotates at the synchronous speed. Let θ be the angular displacement between the *q*-axis and the stator phase *a*-axis, β be the angular displacement between the *q*-axis and the rotor phase *a*-axis circuit. The dq0 reference frame is illustrated in the following figure, where *as* and *ar* represent the stator phase *a*-axis and rotor phase *a*-axis, respectively:

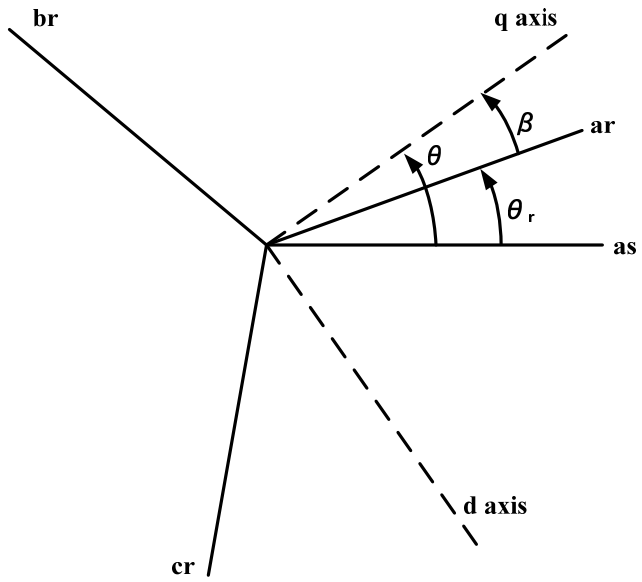

Fig. 2.9. dq0 reference frame

where

$$\theta = \int_0^t \omega_s dt' + \theta(0) \tag{2.19}$$

and

$$\beta = \theta - \theta_r = \int_0^t (\omega_s - \omega_r) dt' + \theta(0) - \theta_r(0) \tag{2.20}$$

θ_r is rotor electrical angular displacement regarding to the stator.

The transformation matrix for the stator quantities is as follows:

$$\mathbf{K_s} = \frac{2}{3}\begin{bmatrix} \cos(\theta) & \cos(\theta - \frac{2\pi}{3}) & \cos(\theta + \frac{2\pi}{3}) \\ \sin(\theta) & \sin(\theta - \frac{2\pi}{3}) & \sin(\theta + \frac{2\pi}{3}) \\ \frac{1}{2} & \frac{1}{2} & \frac{1}{2} \end{bmatrix} \tag{2.21}$$

Similarly, the transformation for the rotor quantities (into the same reference frame) will be as follows.

$$\mathbf{K_r} = \frac{2}{3}\begin{bmatrix} \cos(\beta) & \cos(\beta - \frac{2\pi}{3}) & \cos(\beta + \frac{2\pi}{3}) \\ \sin(\beta) & \sin(\beta - \frac{2\pi}{3}) & \sin(\beta + \frac{2\pi}{3}) \\ \frac{1}{2} & \frac{1}{2} & \frac{1}{2} \end{bmatrix} \tag{2.22}$$

The following equations demonstrate the relationship between *dq0* and *abc* quantities for stator and rotor, respectively:

$$\mathbf{f}_{qd0\mathbf{s}} = \mathbf{K_s}\mathbf{f}_{abc\mathbf{s}} \tag{2.23}$$

$$\mathbf{f}_{qd0\mathbf{r}} = \mathbf{K_r}\mathbf{f}_{abc\mathbf{r}} \tag{2.24}$$

where f is defined as below:

$$\mathbf{f}_{qd\mathbf{o}} = \begin{bmatrix} f_q \\ f_d \\ f_0 \end{bmatrix} \tag{2.25}$$

and

$$\mathbf{f}_{\mathbf{abc}} = \begin{bmatrix} f_a \\ f_b \\ f_c \end{bmatrix} \tag{2.26}$$

According to equations (2.21), (2.22), (2.23) and (2.24), zero–component may be calculated as follows:

$$f_0 = \frac{1}{3}(f_a + f_b + f_c) \tag{2.27}$$

It can be noted that the zero-component is zero for symmetrical *abc*-quantities.

The following equations are used to derive the *dq* components of voltages, currents and flux linkages:

$$\mathbf{K}_\mathbf{s}^{-1}\mathbf{v}_{qd0\mathbf{s}} = R_s\mathbf{K}_\mathbf{s}^{-1}\mathbf{i}_{qd0\mathbf{s}} + \frac{d(\mathbf{K}_\mathbf{s}^{-1}\boldsymbol{\lambda}_{qd0\mathbf{s}})}{dt} \tag{2.28}$$

$$\mathbf{K}_\mathbf{r}^{-1}\mathbf{v}_{qd0\mathbf{r}} = R_r\mathbf{K}_\mathbf{r}^{-1}\mathbf{i}_{qd0\mathbf{r}} + \frac{d(\mathbf{K}_\mathbf{r}^{-1}\boldsymbol{\lambda}_{qd0\mathbf{r}})}{dt} \tag{2.29}$$

$$\mathbf{K}_\mathbf{s}^{-1}\boldsymbol{\lambda}_{qd0\mathbf{s}} = \mathbf{L}_\mathbf{s}\mathbf{K}_\mathbf{s}^{-1}\mathbf{i}_{qd0\mathbf{s}} + \mathbf{L}_\mathbf{m}\mathbf{K}_\mathbf{r}^{-1}\mathbf{i}_{qd0\mathbf{r}} \tag{2.30}$$

$$\mathbf{K}_\mathbf{r}^{-1}\boldsymbol{\lambda}_{qd0\mathbf{r}} = \mathbf{L}_\mathbf{r}\mathbf{K}_\mathbf{r}^{-1}\mathbf{i}_{qd0\mathbf{r}} + \mathbf{L}_\mathbf{m}\mathbf{K}_\mathbf{s}^{-1}\mathbf{i}_{qd0\mathbf{s}} \tag{2.31}$$

Multiplying both sides of equations (2.28) and (2.30) by $\mathbf{K_s}$ and of equations (2.29) and (2.31) by $\mathbf{K_r}$, one can obtain the following results.

$$\mathbf{v}_{qd0s} = R_s \mathbf{i}_{qd0s} + \mathbf{K}_s \frac{d(\mathbf{K}_s^{-1}\boldsymbol{\lambda}_{qd0s})}{dt} \tag{2.32}$$

$$\mathbf{v}_{qd0r} = R_r \mathbf{i}_{qd0r} + \mathbf{K}_r \frac{d(\mathbf{K}_r^{-1}\boldsymbol{\lambda}_{qd0r})}{dt} \tag{2.33}$$

$$\boldsymbol{\lambda}_{qd0s} = \mathbf{K}_s \mathbf{L}_s \mathbf{K}_s^{-1} \mathbf{i}_{qd0s} + \mathbf{K}_s \mathbf{L}_m \mathbf{K}_r^{-1} \mathbf{i}_{qd0r} \tag{2.34}$$

$$\boldsymbol{\lambda}_{qd0r} = \mathbf{K}_r \mathbf{L}_r \mathbf{K}_r^{-1} \mathbf{i}_{qd0r} + \mathbf{K}_r \mathbf{L}_m \mathbf{K}_s^{-1} \mathbf{i}_{qd0s} \tag{2.35}$$

This can be re-written as follows:

$$v_{ds} = R_s i_{ds} + \frac{d\lambda_{ds}}{dt} - \omega_s \lambda_{qs} \tag{2.36}$$

$$v_{qs} = R_s i_{qs} + \frac{d\lambda_{qs}}{dt} + \omega_s \lambda_{ds} \tag{2.37}$$

$$v_{dr} = R_r i_{dr} + \frac{d\lambda_{dr}}{dt} - (\omega_s - \omega_r)\lambda_{qr} \tag{2.38}$$

$$v_{qr} = R_r i_{qr} + \frac{d\lambda_{qr}}{dt} + (\omega_s - \omega_r)\lambda_{dr} \tag{2.39}$$

$$\lambda_{ds} = (L_{ls} + L_M) i_{ds} + L_M i_{dr} \tag{2.40}$$

$$\lambda_{qs} = (L_{ls} + L_M) i_{qs} + L_M i_{qr} \tag{2.41}$$

$$\lambda_{dr} = (L_{ls} + L_M) i_{dr} + L_M i_{ds} \tag{2.42}$$

where

$$L_M = \frac{3}{2} L_{ms} \tag{2.43}$$

The real and reactive stator input powers can be calculated using the following equations (neglecting the power losses associated with the stator resistances) [15, 25]:

$$P_s = \frac{3}{2}(v_{ds} i_{ds} + v_{qs} i_{qs}) \tag{2.44}$$

$$Q_s = \frac{3}{2}(v_{qs} i_{ds} - v_{ds} i_{qs}) \tag{2.45}$$

In this chapter, fundamental concepts of wind energy conversion systems were represented. Among different types of the described wind energy conversion systems, the

DFIG conversion system was described in more detail. The aerodynamical, mechanical, and generator modeling concepts were discussed. In the next chapter, the power electronic ac/ac converter and the corresponding control schemes will be under focus.

Chapter 3

DFIG Wind Energy Conversion Systems

Circuits and Control Schemes

In this chapter, the power electronic circuits used in DFIG wind energy conversion systems are described, and the control schemes are presented. In Section 3.1 the static frequency converter is introduced. Different types of static frequency converters used in DFIG wind energy conversion systems are described among which the back-to-back PWM power electronic converter and its corresponding modulation schemes are discussed in more detail.

Section 3.2 is dedicated to DFIG wind energy conversion systems control schemes: in Section 3.2.1 the back-to-back PWM power electronic converter control schemes are described, and the wind turbine mechanical control scheme is presented in Section 3.2.2

3.1 Static Frequency Converter

A static frequency converter is a power electronic converter that converts the frequency of ac power to the desired value while the output voltage magnitude and phase angle can be controlled. This type of power electronic converter is an essential component of DFIG wind energy conversion system, as it enables the doubly-fed induction generator to operate at different rotor speed values including both sub-synchronous and super-synchronous speed ranges while the stator output power is maintained at the network frequency. [16, 17]

There are two popular topologies for static frequency converters in DFIG systems: single-stage (direct topology) in which energy is directly converted from ac to ac, and double-stage (indirect topology or back-to-back converter), where the first stage provides ac to dc conversion (rectification) and the second stage provides dc to ac conversion (inversion) [18].

A single-stage static frequency changer may use semi-controlled power electronic switches (thyristors) or fully-controlled power electronic switches. The first type is referred to as a naturally commutated cycloconverter, featuring restricted frequency conversion, and the second type is referred to as a forced commutated cycloconverter or a matrix converter [17, 19].

In a double-stage converter, ac power is first converted to dc power and then converted to ac power at the desired frequency. A dc link between the two ac/dc and

dc/ac converters can be used to decrease ripples on the dc voltage. The double-stage converter with a large dc-link capacitor (back-to-back PWM converter) is the most popular ac/ac power electronic converter configuration used in variable-speed wind turbine systems due to its several advantages as listed below:

- Operation at sub-synchronous, super-synchronous and synchronous speed while the speed range is only restricted by the rotor voltage ratings of the doubly-fed induction generator.
- Low distortion stator and rotor currents.
- Independent control of the rotor excitation and generator torque
- Control of the displacement factor between the voltage and the current in the grid-side converter [23]

3.1.1 Back-to-Back PWM Converter

The back-to-back PWM (pulse width modulation) converter is a bidirectional power converter including two ac/dc and dc/ac converters connected together via a dc-link consisting of a capacitor. In a DFIG wind energy conversion system, the back-to-back PWM converter is used to connect the rotor circuit to the grid, while the grid-side converter operates in the rectifying mode (ac/dc), while the rotor-side converter operates in the inverting mode (dc/ac). The two converters make use of insulated gate bipolar transistors (IGBT) provided with freewheeling diodes. The schematic diagram of the back-to-back PWM converter is illustrated in Fig. 3.1.

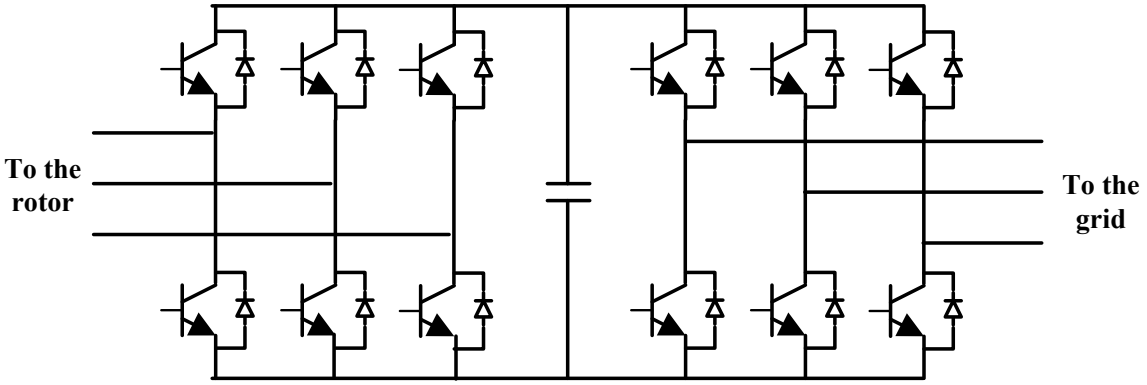

Fig. 3.1. Back-to-back PWM converter

It is worth mentioning that in order to achieve full control of the current injected into the grid, the dc-link voltage will be maintained at a level higher than the amplitude of the grid line-to-line voltage. This should be considered in determination of the dc-link capacitor ratings.

3.1.2 Back-to-Back PWM Converter Modulation Schemes

There are several modulation techniques for the inverter and rectifier sides of the back-to-back PWM converter among which two commonly used modulation techniques, sinusoidal pulse-width modulation (SPWM) and optimized pulse-width modulation (OPWM) schemes are described in this section and are used in this research.

3.1.2.1 Sinusoidal Pulse Width Modulation (SPWM)

In SPWM scheme, the firing pulses of the power electronic switches (i.e. IGBTs for the back-to-back SPWM converters) are generated in a way that the fundamental component of the output voltage has the desired magnitude and phase.

In carrier-based SPWM, a sinusoidal reference signal is compared to a high frequency triangular signal in order to generate the firing pulses for the power electronic switches. The triangular signal should have a period much smaller than the smallest time constant of the system [20]. The firing pulse, S, is generated as below:

$$S = \begin{cases} 1 & if\ carrier < ref \\ 0 & if\ carrier > ref \end{cases}$$

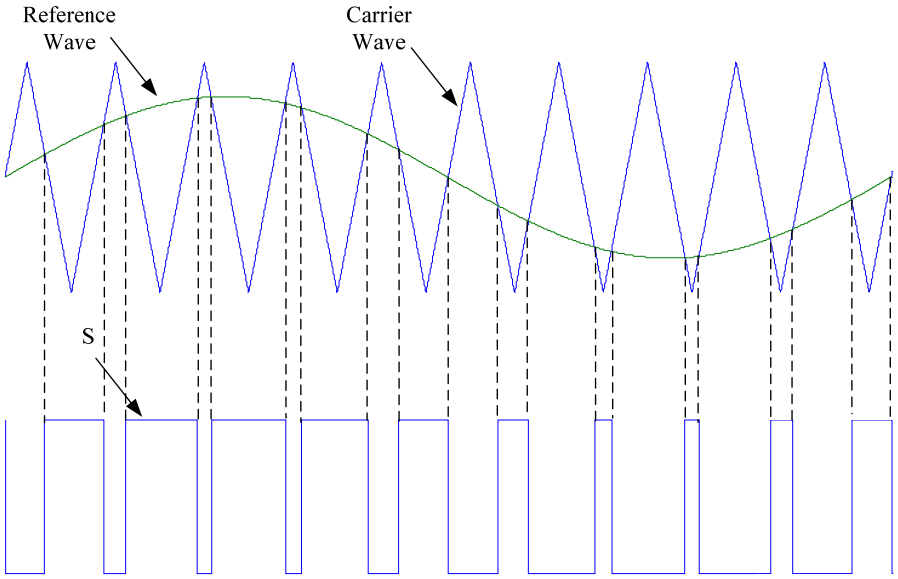

Fig. 3. 2. SPWM scheme (Adopted from [21])

In a three-phase SPWM controller, the reference signal corresponding to each leg of the converter is separately generated in a way that each is 120˚ apart from the other one. The output is a three-phase voltage, and the fundamental components of the three-phase output voltage are shifted by 120˚ [22]. The ratio of the output signal fundamental component to half of the dc bus voltage is referred to as modulation index, m, and is given as follows:

$$m = \frac{V_{\max}}{\frac{E}{2}} \tag{3.1}$$

In this research, for SPWM scheme, the frequency ratio of the carrier waveform to the reference waveform is 27.

3.1.2.2 Optimal Pulse Width Modulation (OPWM)

In OPWM scheme, a system of nonlinear simultaneous equations to calculate the firing angles is solved offline in order to eliminate the most significant harmonics and set the fundamental component of ac output to a given value. In this type of modulation, the switching rate is greatly decreased compared to SPWM scheme. The magnitude of h^{th} harmonic, V_h, can be derived from the following equation:

$$V_h = \frac{4E}{h\pi}(1 - 2\cos(h\alpha_1) + 2\cos(h\alpha_2) - 2\cos(h\alpha_3) + ...) \tag{3.2}$$

where α_i represents the i^{th} switching angle[22].

Using equation (3.2), a system of equations can be solved to obtain a set of firing angles that will result in a given frequency spectrum. An example of an OPWM output with the corresponding fundamental component wave is illustrated in the figure below.

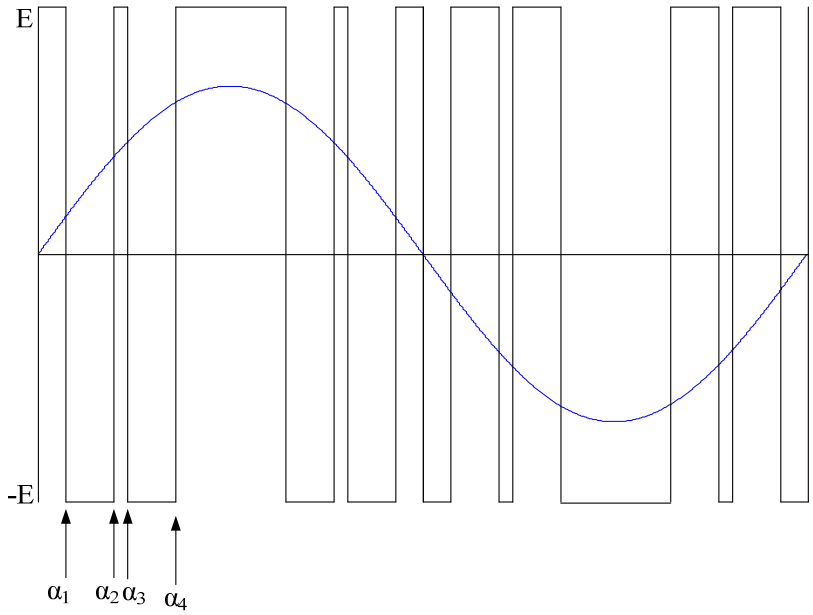

Fig. 3. 3. OPWM scheme (Adopted from [21])

In this research the OPWM switching scheme has five switching angles.

3.2 DFIG Wind Energy Conversion Systems Control Schemes

In this section, the control systems including electrical and mechanical control schemes for DFIG wind energy conversion systems are presented. The electrical control deals with controlling the back-to-back PWM converter, while mechanical control is

designed in a way that the wind turbine captures the optimum mechanical power from blowing wind.

3.2.1 Back-to-Back PWM Converter Control Schemes

In this section, detailed control schemes for the grid-side and rotor-side converters for the back-to-back PWM converter are presented. These control schemes use vector control approach, which was described earlier in Chapter 2 with a reference frame oriented along the stator flux vector position. The objective of the grid-side converter (GSC) control is to regulate the dc-bus voltage, and to control the reactive power exchange between the rotor and the grid. The rotor-side converter (RSC) controller is used to regulate the doubly-fed induction generator rotor speed, and the stator reactive power. A DFIG wind energy conversion system is illustrated in Fig. 3.4.

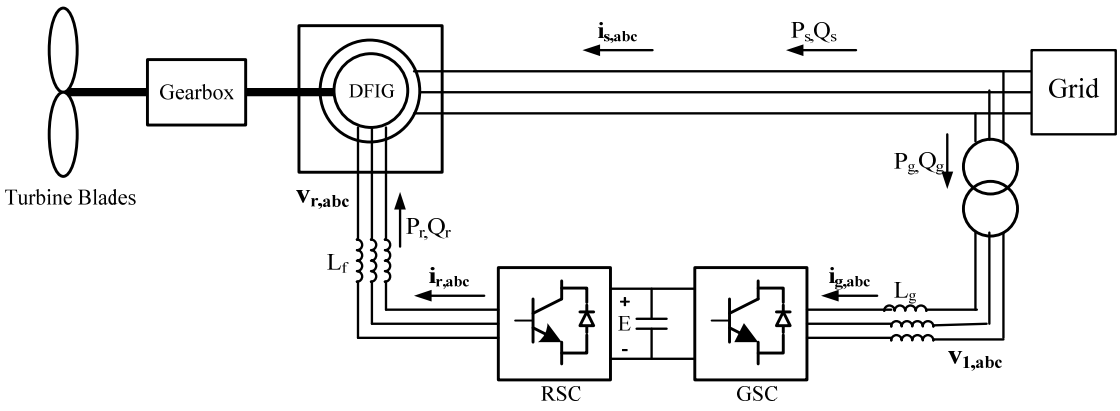

Fig. 3.4. DFIG wind energy conversion system

- **Rotor Side Converter Control**

In *dq* conversion, if the *d*-axis of the selected reference frame is aligned with the stator flux linkage vector, the *q*-component of stator flux linkage will be zero (λ_{qs}=0, and λ_{ds}=λ_s). This in combination of Equations (2.37), (2.40), and (2.41) results in the following equations for *d* and *q* components of stator current:

$$i_{qs} = \frac{-L_M i_{qr}}{L_{ls} + L_M} \tag{3.3}$$

$$i_{ds} = \frac{L_M (i_{ms} - i_{dr})}{L_{ls} + L_M} \tag{3.4}$$

where

$$i_{ms} = \frac{v_{qs} - R_s i_{qs}}{\omega_s L_M} \tag{3.5}$$

Equations (2.38) and (2.39) can be rewritten as follows:

$$v_{dr} = \underbrace{R_r i_{dr} + \sigma(L_{lr} + L_M)\frac{di_{dr}}{dt}}_{v_{dr1}} - (\omega_s - \omega_r)\sigma(L_{lr} + L_M) i_{qr} \tag{3.6}$$

$$v_{qr} = \underbrace{R_r i_{qr} + \sigma(L_{lr} + L_M)\frac{di_{qr}}{dt}}_{v_{qr1}} + (\omega_s - \omega_r)\left(\frac{\sigma(L_{lr} + L_M) i_{dr} + L_M^2 i_{ms}}{L_{ls} + L_M}\right) \tag{3.7}$$

where

$$\sigma = 1 - \frac{L_M^2}{(L_{ls} + L_M)(L_{lr} + L_M)} \tag{3.8}$$

Electric torque and stator reactive power can be calculated as follows [17]:

$$T_e = \left(\frac{-L_M i_{ms} i_{qr}}{L_{ls} + L_M}\right) \tag{3.9}$$

$$Q_s = \frac{3}{2}\frac{\omega_s L_M^2 i_{ms}(i_{ms} - i_{dr})}{L_{ls} + L_M} \tag{3.10}$$

According to Equations (2.1), (3.9) and (3.10), the rotor speed, ω_r, and the stator reactive power, Q_s, can be controlled using the rotor current *q*-component, i_{qr}, and the rotor current *d*-component, i_{dr}, respectively. In others words, the reference value for the rotor speed, $\omega_{r,ref}$, and the stator reactive power, Q_{ref}, can be used to calculate the reference values for the rotor current *q*-component and the rotor current *d*-component, respectively.

According to Equations (3.6) and (3.7), i_{dr} and i_{qr} can be used to obtain v_{dr1} and v_{qr1}, respectively. v_{dr} can be calculated using v_{dr1} and i_{qr}, and v_{qr} can be calculated using v_{qr1} and i_{dr}.

The overall control block diagram of rotor-side converter is illustrated in Fig. 3.5:

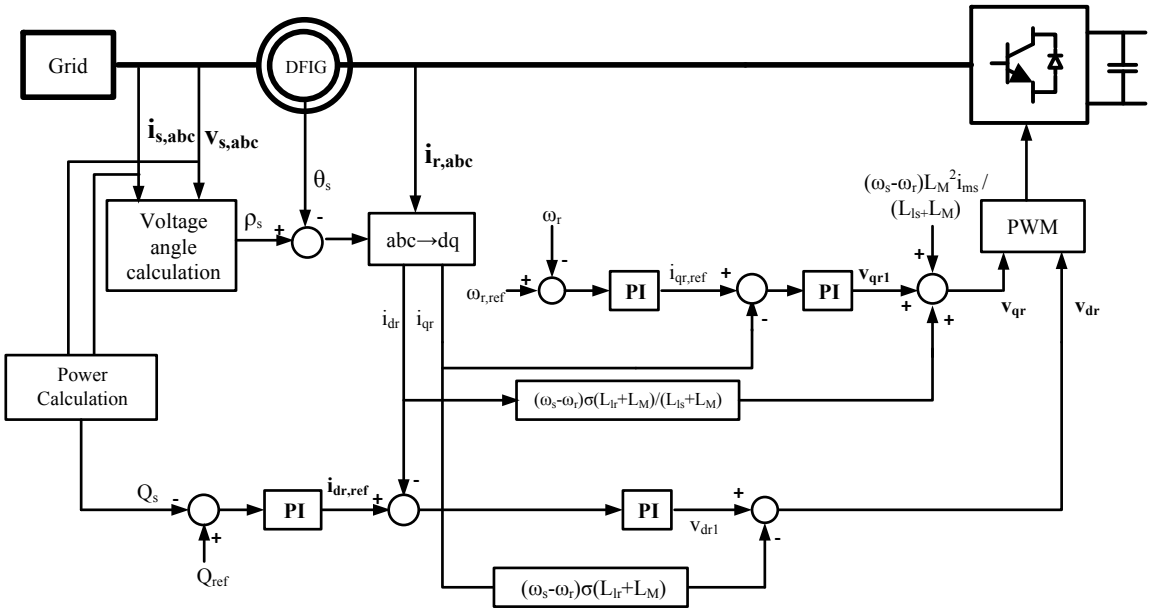

Fig. 3.5. Rotor-side converter control scheme

- **Grid-side Converter Control**

As mentioned previously, the aim of the grid-side converter controller is to keep the dc-bus voltage constant, and to control the reactive power flowing between the rotor and the grid.

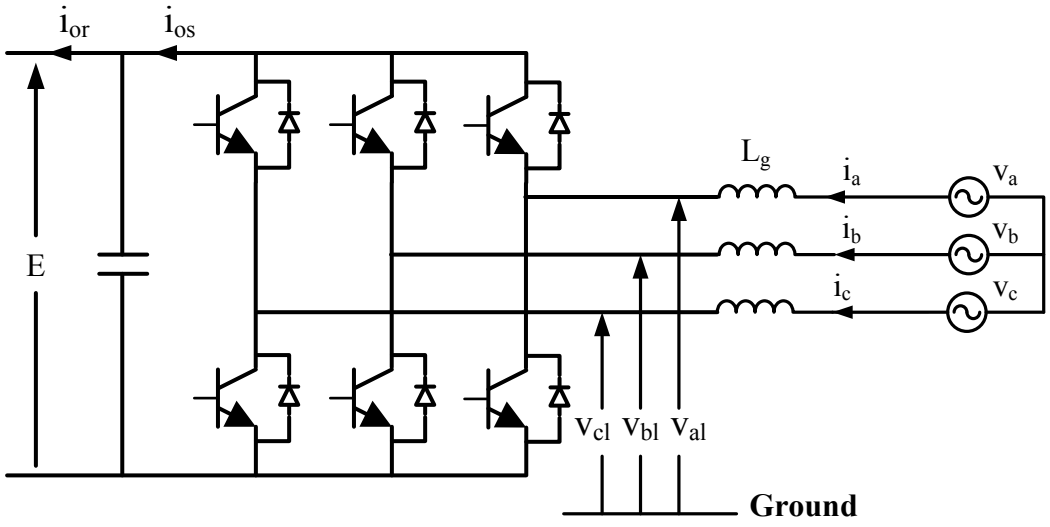

Fig. 3. 6. Grid-side converter model

Real and reactive power flowing from the grid to the rotor circuit can be defined using *dq* components as below:

$$P_g = \frac{3}{2}(v_{dl} i_{dg} + v_{ql} i_{qg}) \tag{3.11}$$

$$Q_g = \frac{3}{2}(v_{ql} i_{dg} - v_{dl} i_{qg}) \tag{3.12}$$

where v_{dl} and v_{ql} represent the *d*-components and the *q*-component of the grid voltage, respectively, and i_{dg} and i_{qg} represent the *d*-components and the *q*-component of the input current of the GSC.

If the *d*-axis of *dq* frame is aligned with the stator voltage position, the *q*-component of stator voltage is equal to zero ($v_{ql} = 0$), and the *d*-component of stator voltage (v_{dl}) is constant. Therefore, the reactive power can be controlled via i_{qg} according to the equation below:

$$Q_g = -\frac{3}{2} v_{dl} i_{qg} \tag{3.13}$$

Neglecting the small power loss in power electronic switches, P_q can be calculated as

$$P_g = E i_{os} \tag{3.14}$$

Using Equations (3.11) and (3.14), the following equation can be obtained.

$$E i_{os} = \frac{3}{2} v_{dl1} i_{dg} \tag{3.15}$$

where v_{dl1} represents the *d*-component of the converter grid-side voltage.

Neglecting the harmonics due to switching, one can write the following equations for the rotor-side converter circuit:

$$v_{dl1} = \frac{m_g}{2\sqrt{2}} E \tag{3.16}$$

According to (3.15) and (3.16), i_{os} can be controlled using i_{dg}.

$$i_{os} = \frac{3 m_g}{2\sqrt{2}} i_{dg} \tag{3.17}$$

The relationship between E and i_{os} can be described as follows.

$$C \frac{dE}{dt} = i_{os} - i_{or} \tag{3.18}$$

where m_g represent the modulation index for the grid-side converter [24].

Equation (3.18) suggests that the dc link voltage can be controlled via i_{dg}.

The next step would be to derive the values of the *d* and *q* components of the converter grid-side voltage (v_{dl1} and v_{ql1}). For this purpose, the following equations can be used:

$$v_{dl1} = v_{dl} - R i_{dg} - L_g \frac{d i_{dg}}{dt} + \omega_e L_g i_{qg} \tag{3.19}$$

$$v_{ql1} = v_{ql} - Ri_{qg} - L_g \frac{di_{qg}}{dt} - \omega_e L_g i_{qg} \tag{3.20}$$

Proportional-integral (PI) controllers can be used to control the values of v_{dl1} and v_{ql1} using i_{dg} and i_{qg}. The overall control block diagram for the grid-side converter is illustrated in the figure below, in which the reference value of the reactive power flowing from the grid to the converter and the reference value of dc-link voltage are used to calculate the *d* and *q* components of the converter grid-side voltage:

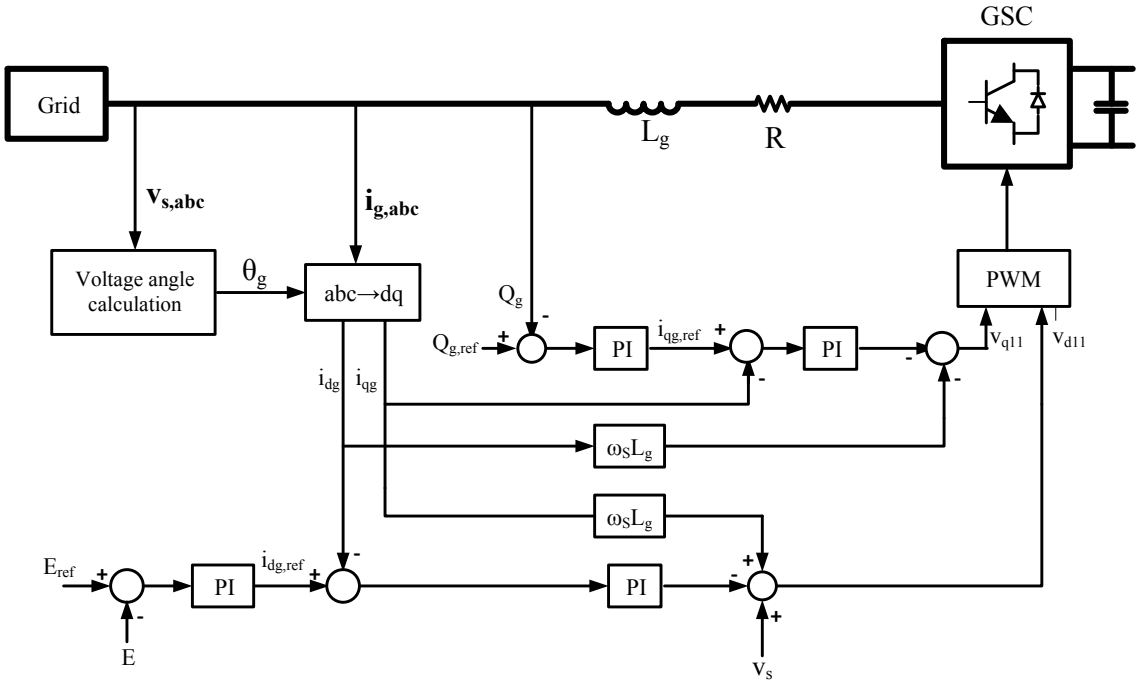

Fig. 3.7. Grid-side converter control block diagram

In this research, the electromagnetic transient (EMT) simulation software PSCAD/EMTDC is used for simulation. The DFIG wind energy conversion system as illustrated in Fig. 3.4 is simulated in PSCAD/EMTDC. The back-to-back PWM converter is simulated under both SPWM and OPWM schemes. Some technical data for the DFIG examined in the research describe in this thesis are provided in Table 3.1.

DFIG specifications		
Rated power	1	MW
Rated voltage	0.69	kV
Rated current	0.836	kA
Stator resistance	0.0054	pu
Wound rotor resistance	0.0061	pu
Magnetizing inductance	4.5	pu
Stator leakage inductance	0.1	pu
Wound rotor leakage inductance	0.011	pu
Stator/rotor turns ratio	0.3	
Mechanical damping	0.0001	N.m/rad/s

Table 3.1. DFIG rating specifications used in simulation

The simulation results are demonstrated below for SPWM and OPWM schemes, respectively. The simulation time step is 5 μs. The reference value for each of the variables is demonstrated on the corresponding graph as well.

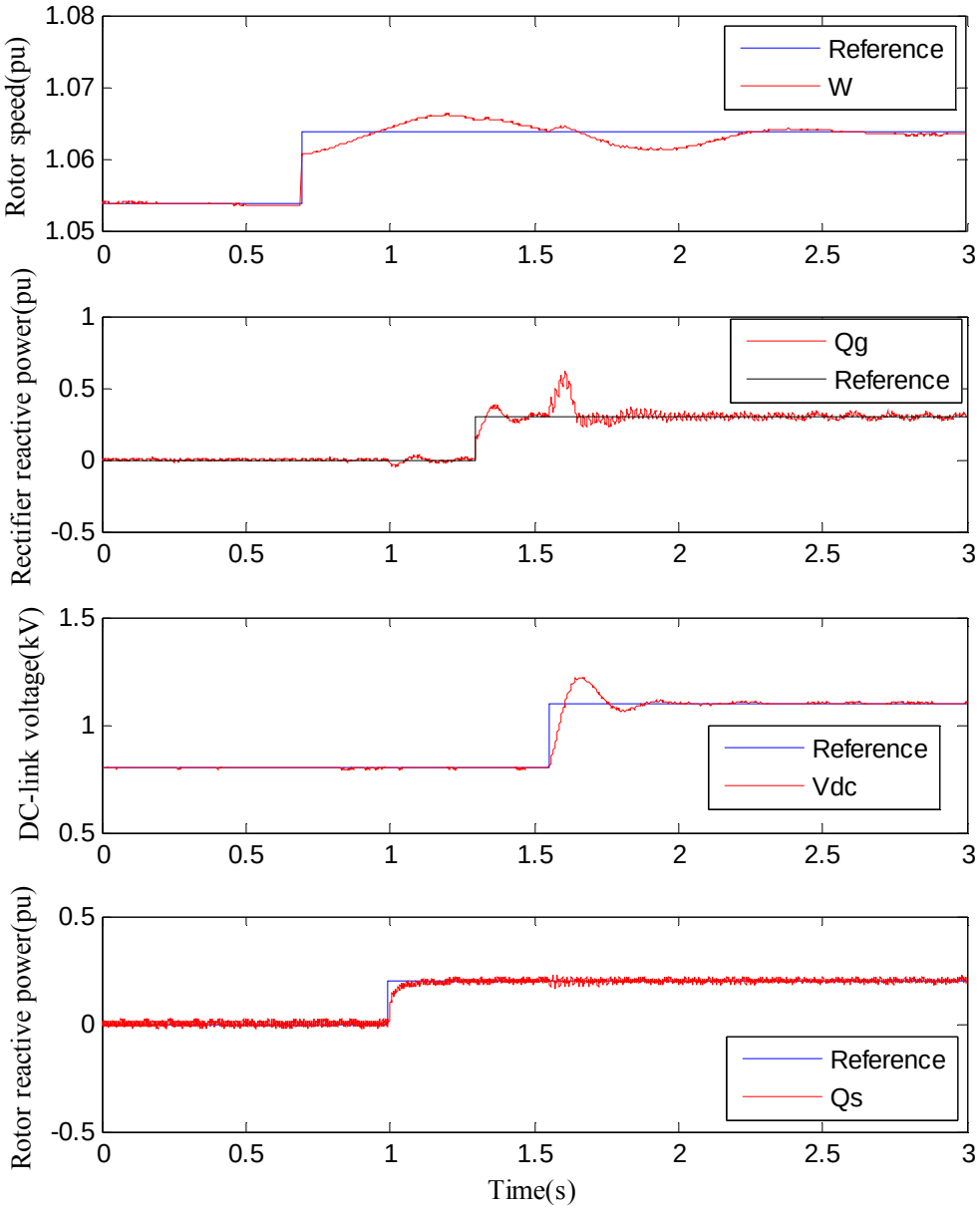

Fig. 3. 8. DFIG wind energy conversion system with SPWM scheme

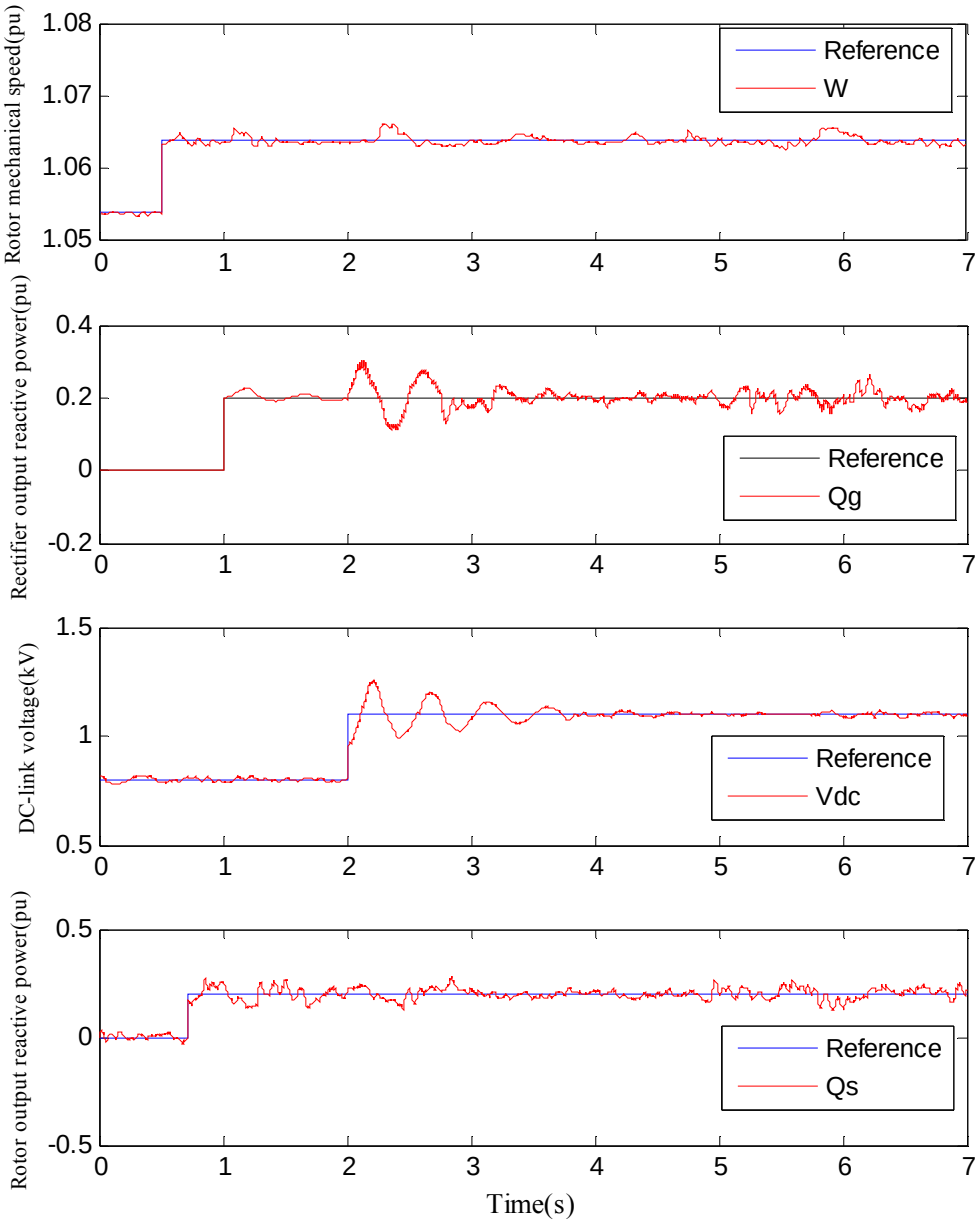

Fig. 3. 9. DFIG wind energy conversion system with OPWM scheme

3.2.2 Mechanical Control

The mechanical power captured from wind energy is a function of turbine shaft angular speed. In order to maximize the captured mechanical power, the turbine shaft angular speed should be maintained at an optimum level, which is determined based on the wind turbine operating region.

In this section, different operating regions for the wind turbine are described, and corresponding control methods for the wind turbine shaft angular speed (also referred to as maximum power point tracking (MPPT) methods) are presented.

3.2.2.1 Wind Turbine Operating Regions

As the wind speed increases, the turbine shaft rotational speed increases, and the wind turbine input mechanical power changes. Fig. 3. 10. illustrates the change of mechanical power with turbine shaft rotational speed variation at different wind velocities. The optimum power point for different wind velocities are demonstrated in the figure as well.

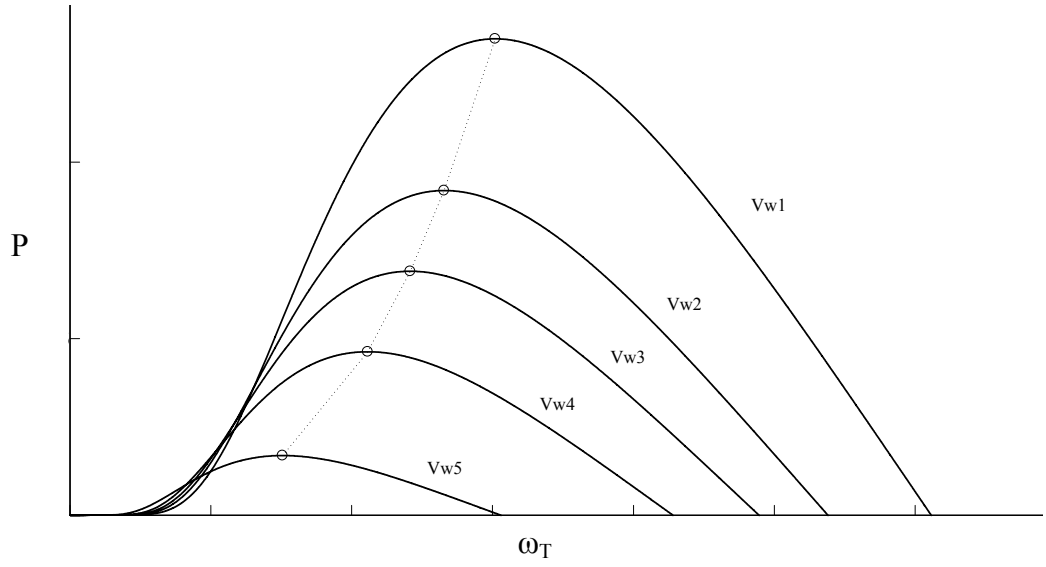

Fig. 3. 10. Wind turbine characteristics with $V_{w1}>V_{w2}>V_{w3}>V_{w4}>V_{w5}$

As discussed earlier in Chapter 2, at a given wind velocity, the mechanical power extracted from wind is a function of turbine shaft rotational speed and the pitch angle. Therefore, to control and maximize the mechanical extracted power it is necessary to control the turbine shaft angular speed and the pitch angle. The turbine shaft angular speed is controlled through the rotor-side converter controllers, and there is a pitch angle controller to adjust the pitch angle. However, the latter is only active in high wind speeds.

For different values of wind speed, turbine shaft angular speed and mechanical power extracted from wind, four main operating regions for the wind turbine can be defined; each operating region has its corresponding control methods. The main operating regions of a wind turbine are illustrated in Fig. 3.11 [10], [19].

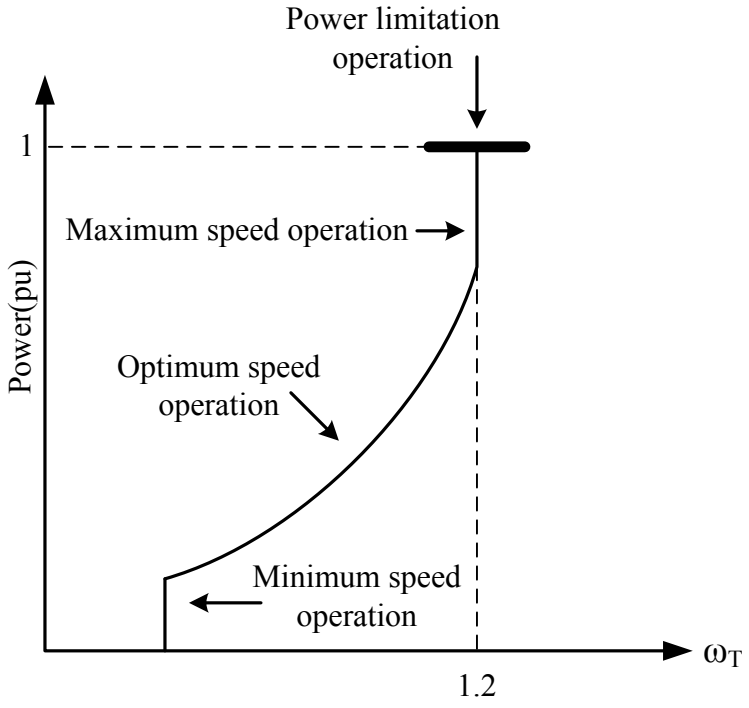

Fig. 3.11. Wind turbine operating regions

- **Minimum Speed Operating Region:**

This operation region is selected when wind speed is low. In this region, the shaft angular speed is kept constant at its minimum value, which is usually around 25%-30% below synchronous speed.

- **Optimum Speed Operating Region:**

In this region, the wind turbine operates at optimal power tracking point according to the wind speed. The shaft angular speed is controlled via the rotor-side converter in order to work at the optimal power point and extract maximum power from the wind.

- **Maximum Speed Operating Region:**

When wind speed is high, the turbine shaft angular speed should be controlled in order not to exceed a certain limit (usually 20% above the synchronous speed). In this region, the extracted mechanical power is not at its optimal point anymore. The speed is still controlled via the rotor-side converter speed controller.

- **Power Limitation Operating Region**

With excessively high wind speed, the rotor-side converter is no longer able to keep the speed constant at its maximum value. At this region, speed is controlled via a pitch angle controller. The pitch angle controller adjusts pitch angle in order to reduce the extracted mechanical power, and keeps the shaft angular speed constant at its maximum value.

3.2.2.2 Wind Speed Measurement Method

As discussed earlier, in the optimum speed operation region, the shaft angular speed is controlled via the rotor-side converter controllers. There are several maximum power point tracking (MPPT) methods to determine the reference value for shaft angular speed, such as Perturbation and Observation Method, Wind Speed Measurement Method, and Power Signal Feedback (PSF) Control. In this section, Wind Speed Measurement Method is described.

This method computes the optimal tip-speed ratio, λ_{opt}, and therefore the reference value for turbine shaft rotational speed for a given wind speed. In this method, wind

speed and shaft angular speed are measured, and the optimal tip-speed ratio is determined for the corresponding wind speed using look-up tables. The reference shaft angular speed can calculated based on the equation below:

$$\omega_{T,ref} = \frac{v_w \lambda_{opt}}{R} \tag{3.21}$$

The reference value is used in then rotor-side converter control system to adjust the turbine shaft angular speed.

In this chapter the back-to-back PWM power electronic converter and two types of modulation schemes (SPWM and OPWM) were described. Also, the control schemes of the power electronic converter and the mechanical control of the wind turbine were explained. In the next chapter, two types of reduced intensity modeling techniques for the back-to-back PWM converter are described and applied to the DFIG wind energy conversion system simulation model.

Chapter 4

Back-to-Back PWM Converter Modeling

In order to design and verify the performance of a wind energy generation system, it is necessary to simulate the wind farm. Conventional detailed simulation models, e.g. electromagnetic transient (EMT) simulation models, which include all corresponding power electronic switches provide accurate results. However, there are a number of difficulties in using the detailed model due to presence of power electronic switches.

There are numerous wind energy generators in a wind farm and each wind energy generator has its corresponding ac/ac power electronic converter. The system topology in a detailed model of the wind generation system changes frequently due to power electronic converter switchings. Therefore, simulation of a wind

farm using the detailed model tends to be time consuming and computationally intensive; in fact, it may sometimes be impractical when the simulation results are needed in a limited time. In this chapter, two approaches are used to ease the simulation of power electronic converter's detailed model. The first approach is to use dependent voltage and current sources instead of actual power electronic switches, and is referred to as the switching-function model. The second approach is to use the average value of signals instead of exact values, and is referred to as the dynamic average-value model.

In this chapter, the two reduced intensity models and their applications to the DFIG wind energy conversion system simulation are described. The detailed simulation results are provided to verify the accuracy of the models. The simulations run time of the reduced intensity models for one DFIG are recorded and compared to the detailed EMT model. Also, these models are applied to a small representative test system connected to a wind farm consisting of DFIGs. The simulation results show that both approaches result in reduction in simulation execution time.

4.1 Switching- Function Model

In computer simulation using the detailed EMT model, in every switching instant the topology of the system changes. Consequently the system admittance matrix changes. This tends to slow down the simulation speed.

The idea behind the switching-function model is to keep the system topology constant, which helps reduce the simulation run time. In this approach all the switching

instants are calculated in a similar way as the detailed model. Instead of using actual power electronic switches, an equivalent circuit of the rectifier/inverter including dependent voltage and current sources are used in the simulation. The values of the voltage/current of these sources are calculated at every switching time step. In other words, instead of changing system topology at every time step, the changes of voltages/currents due to the switchings are calculated and used for simulation.

In this section, switching-function modeling of the rectifier in the back-to-back PWM converter is represented. This concept can be extended to the inverter as well. After calculation of switching instants according to the corresponding modulation schemes (i.e. SPWM, OPWM), the rectifier can be replaced by a set of dependent voltage and current sources where the amount of voltage/current is calculated using the dc-link actual voltage and 3-phase input currents in every time step. The rectifier and its corresponding switching-function model are illustrated in Fig. 4. 1. and Fig. 4.2., respectively.

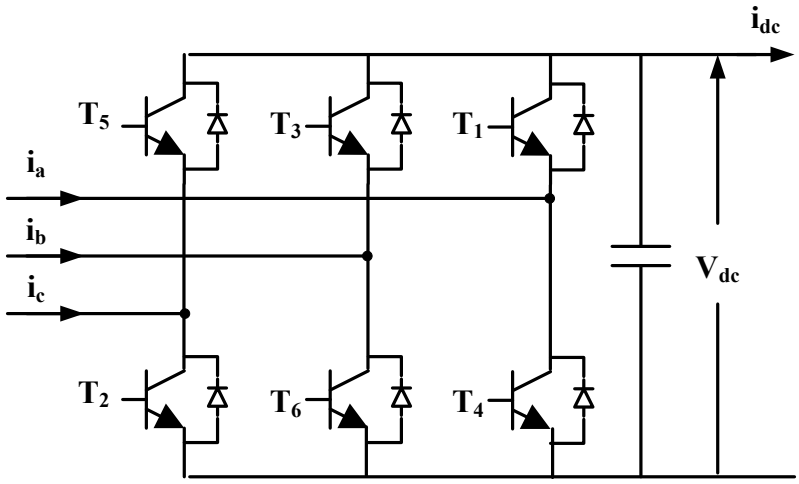

Fig. 4. 1. The rectifier detailed model

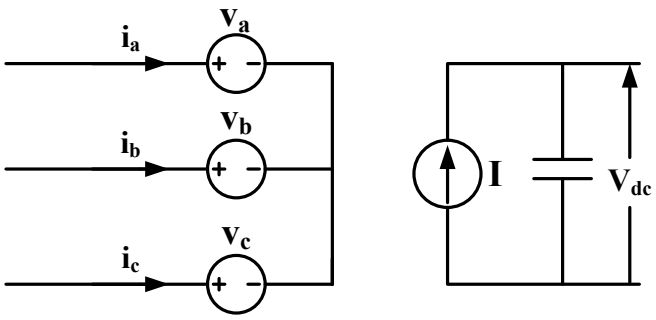

Fig. 4.2. The rectifier equivalent switching-function model

The voltage values for the dependable voltage sources, v_a, v_b, and v_c can be calculated using the switching pulses and the dc voltage as below:

$$\begin{cases} v_a = T_1 V_{dc} - T_4 V_{dc} \\ v_b = T_3 V_{dc} - T_6 V_{dc} \\ v_c = T_5 V_{dc} - T_2 V_{dc} \end{cases} \tag{4.1}$$

where

$$T_i = \begin{cases} 0 & \text{when the switch "i" is off} \\ 1 & \text{when the switch "i" is on} \end{cases} \tag{4.2}$$

The value for the dc current source in the switching-function model can be calculated as:

$$I = T_1 i_a + T_3 i_b + T_5 i_c \tag{4.3}$$

While all the switching pulses are calculated in the same manner as in the detailed model.

This model has been used in PSCAD/EMTDC EMT program to simulate the rectifier of the back-to-back PWM converter. The simulation block in the PSCAD/EMTDC for Fig. 4.2 is illustrated in Fig. 4.3.

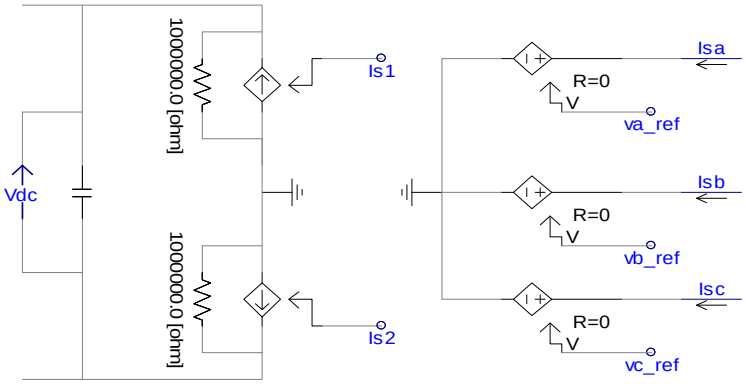

Fig. 4.3. Rectifier switching- function model in PSCAD/EMTDC

Where the signals va_ref, vb_ref, and vc_ref are calculated using the dc link voltage and switching pulses as illustrated in Fig. 4.4. Also, signals Is1 and Is2 are calculated using Isa, Isb, Isc and the switching pulses as illustrated in Fig.4.5.

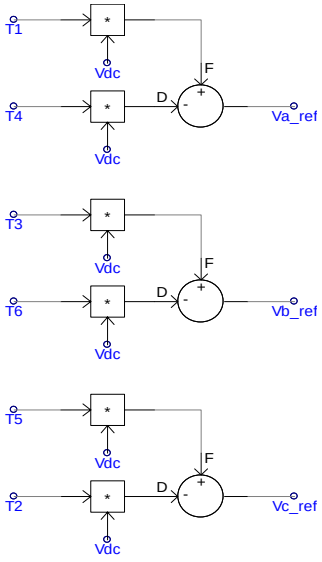

Fig. 4.4. Calculation of voltage sources input values using rectifier switching-function model in PSCAD/EMTDC

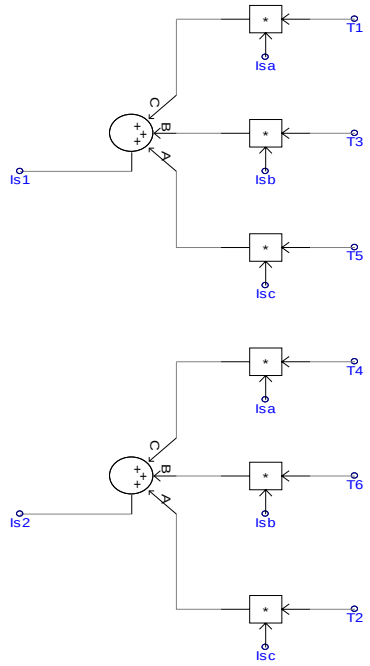

Fig.4.5. Calculation of current sources input values using rectifier switching-function model in PSCAD/EMTDC

This approach is used to reduce the simulation computational time for the simulation of the DFIG wind energy conversion system with specifications stated in Table 3.1 with both SPWM and OPWM schemes. The simulation results obtained using the switching-function models in PSCAD/EMTDC for SPWM and OPWM are illustrated in Fig. 4. 6. and Fig. 4. 7., respectively. In each figure, the results obtained from simulation using the EMT detailed model and the corresponding switching-function model along with the reference values are also included. The simulation time step is 5 μs. As demonstrated in the figures, the results of switching-function models for both SPWM and OPWM schemes are closely similar to the results of the EMT detailed model simulation.

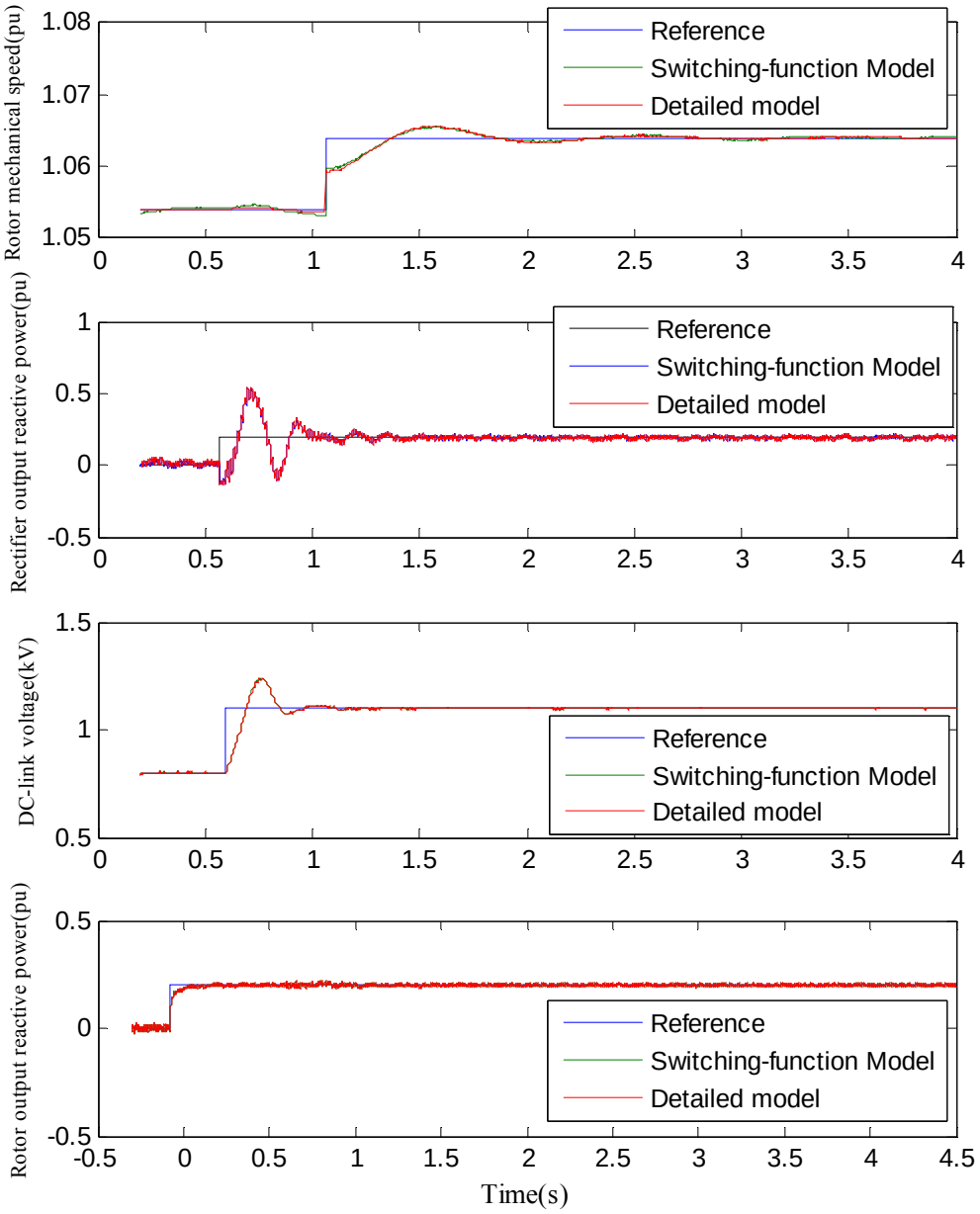

Fig. 4. 6. SPWM modulation, switching-function and detailed model results

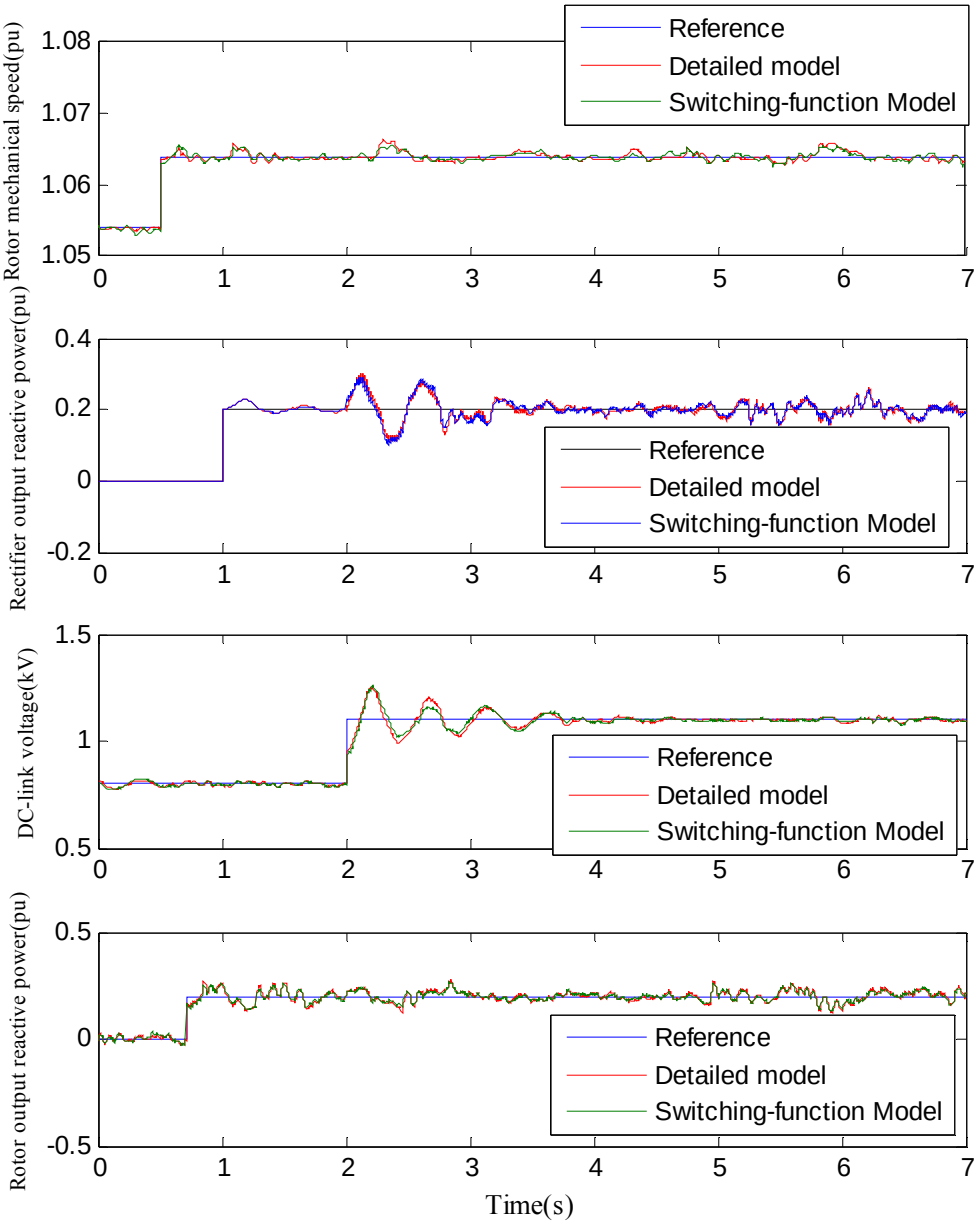

Fig. 4. 7. OPWM modulation, switching-function and detailed model results

To compare the simulation speed of the switching-function model and the EMT detailed model, the actual execution time of simulation for the same simulation run time

(10 seconds) are included in the table below. In the case of OPWM simulation, the switching function model reduces the simulation execution time by 22%, and with SPWM scheme, the switching-function model reduces the simulation execution time by 56%.

	Actual execution time(s)
EMT Detailed OPWM Model	375
Switching- function OPWM model	292
EMT Detailed SPWM Model	704
Switching- function SPWM model	310

Table 4.1. Simulation execution time for switching-function and EMT detailed models

4.2 Dynamic Average-Value Modeling

As mentioned previously, detailed model simulation of wind farms using the actual power electronic switches is time consuming due to the change of the system topology in every switching instant. Another approach to overcome this issue is to obtain a time-invariant circuit topology through "averaging" the power electronic switchings, which is called the dynamic average-value modeling technique. In dynamic average-value

modeling, fast switchings are averaged to simplify and therefore accelerate power electronic converter simulations. In other words, the discontinuous switching cells are replaced with continuous blocks, i.e. voltage and current sources [26], [27]. In average models, some details of the power electronic converter such as higher harmonic contents are eliminated. However, these details are not significantly useful in many cases, and can therefore be ignored.

4.2.1 Dynamic Average-Value Modeling Technique in DFIG Simulation

In this section the dynamic average-value modeling technique for SPWM is described and applied on the back-to-back PWM power electronic converter of a DFIG.

4.2.1.1 Concept of Average-Value Modeling

As mentioned earlier in Chapter 3, in SPWM technique a switching pulse is generated from comparison of a high-frequency triangular waveform with a sinusoidal reference signal. The SPWM scheme and the dynamic average-value outputs are illustrated in Fig. 4. 8. The frequency of the sinusoidal reference signal should be relatively small compared to the triangular waveform frequency. Within a short time period, the sinusoidal waveform can be approximated with a constant value, as illustrated in Fig. 4. 8.

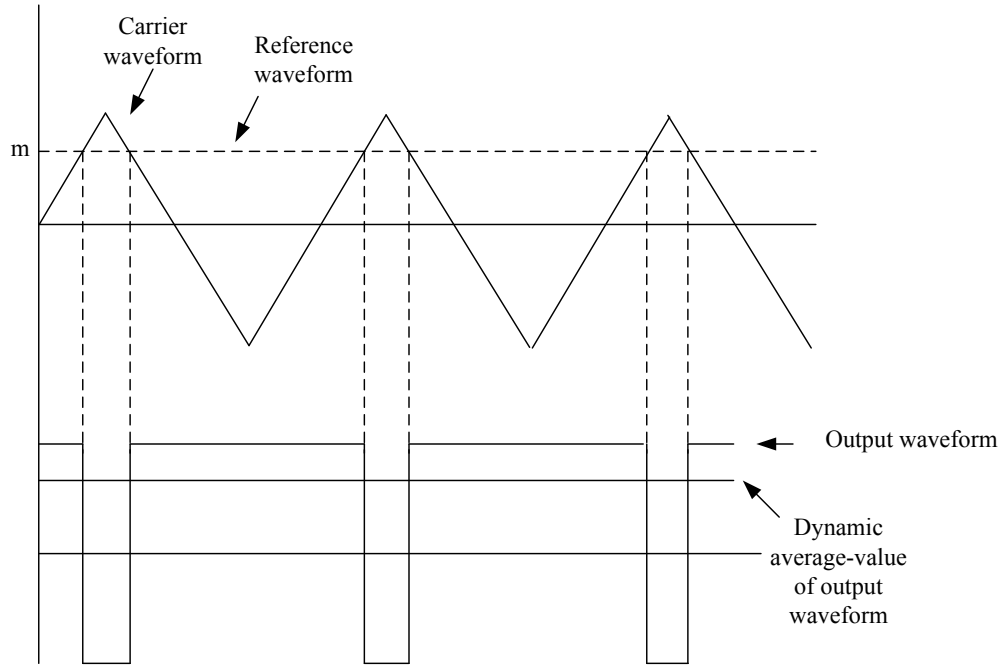

Fig. 4. 8. SPWM scheme and average-value output

The dynamic average-value of a current or voltage waveform represents the dc value of the corresponding variable over a selected time interval, while the ripple is neglected.

$$\bar{x}(t) = \int_{t-T}^{T} x(\tau) d\tau \tag{4.4}$$

where x(t) could represent voltage or current, and T is the switching interval.

It is worth noting that this idea can be extended in a way that the average-value variable includes higher order harmonics, which is essential in resonant converters [27].

The average value of the output ac voltage is illustrated in Fig. 4. 8 as follows:

$$\overline{v_{an}} = \frac{V_{dc}}{2} m_a \tag{4.5}$$

where $\overline{v_{an}}$ and m_a represent the average value of the phase '*a*' output voltage and modulation index, respectively [31].

The same equation is applied to phases *b* and *c*:

$$\overline{v_{bn}} = \frac{V_{dc}}{2} m_b \tag{4.6}$$

$$\overline{v_{cn}} = \frac{V_{dc}}{2} m_c \tag{4.7}$$

where

$\overline{v_{bn}}$ = the average value of the phase '*b*' output voltage

$\overline{v_{cn}}$ = the average value of the phase '*c*' output voltage

m_b = phase '*b*' modulation index

m_c =phase '*c*' modulation index

The modulation indices of the three phases are determined in a way the output phase voltages generate symmetrical three phase voltage. The relationship between the modulation indices of phases *a*, *b*, and *c* is as follow:

$$m_a = m.\cos(\theta) \tag{4.8}$$

$$m_b = m.\cos(\theta - \frac{2\pi}{3}) \tag{4.9}$$

$$m_c = m.\cos(\theta + \frac{2\pi}{3}) \tag{4.10}$$

The average-value concept can also be used in *dq* variables. Using this approach, the *dq* variables will contain a dc value with some ripple, which represents the harmonics. This dc value can be used for average-value modeling [27] [28]. This approach is described and used in details in the next section

4.2.1.2 Application of Average-Value Modeling in DFIG Simulation

In this section, the application of the average-value modeling technique on the rectifier of a back-to-back PWM converter is described. It can be applied on the inverter in a similar approach as well.

It is more convenient to choose the *dq* transformation reference frame in a way that the averaged *d*-component of an ac voltage is zero. This can be accomplished by aligning the *q*-axis of the *dq* reference frame with the voltage. This way, the *d*-axis is perpendicular to the voltage vector, and the *d*-component of the voltage is equal to zero. This *dq* reference frame is referred to as the rectifier reference frame in this section, as this section is dedicated to the average-value modeling of the rectifier of the back-to-back PWM converter.

In the case that an arbitrary *dq* reference frame is used, which does not satisfy the above condition, the *dq* values can be transferred to a *dq* reference frame in which the *q*-axis is aligned with the voltage vector. As illustrated in Fig. 4.9, a transformation angle δ is chosen in a way to make sure $v_d^{rec} = 0$, where superscription *rec* denotes quantities in the rectifier reference frame and the bar represents the average-value evaluated over a

switching interval [22]. Superscript *a* in Fig. 4.9 represents quantities in the arbitrary reference frame.

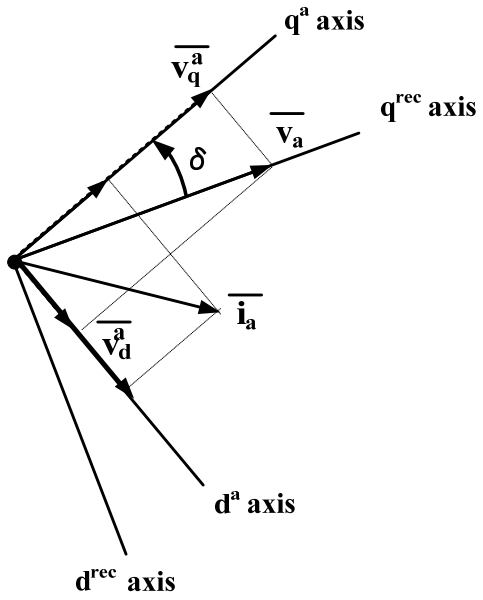

Fig. 4.9. Rectifier average-value voltages and currents in the dq reference frame

The *dq* values from an arbitrary reference frame can be transferred to the rectifier *dq* reference frame as follows [26].

$$\begin{bmatrix} \overline{v_q^{rec}} \\ 0 \end{bmatrix} = \begin{bmatrix} \cos(\delta) & \sin(\delta) \\ -\sin(\delta) & \cos(\delta) \end{bmatrix} \begin{bmatrix} \overline{v_q^a} \\ \overline{v_d^a} \end{bmatrix} \tag{4.11}$$

Using the rectifier *dq* reference frame, the average-value modeling technique can be applied on the rectifier. The switches are replaced by voltage and current source using the average values. The schematic of the rectifier and its corresponding average-value model are illustrated in Fig. 4. 10 and Fig. 4. 11, respectively.

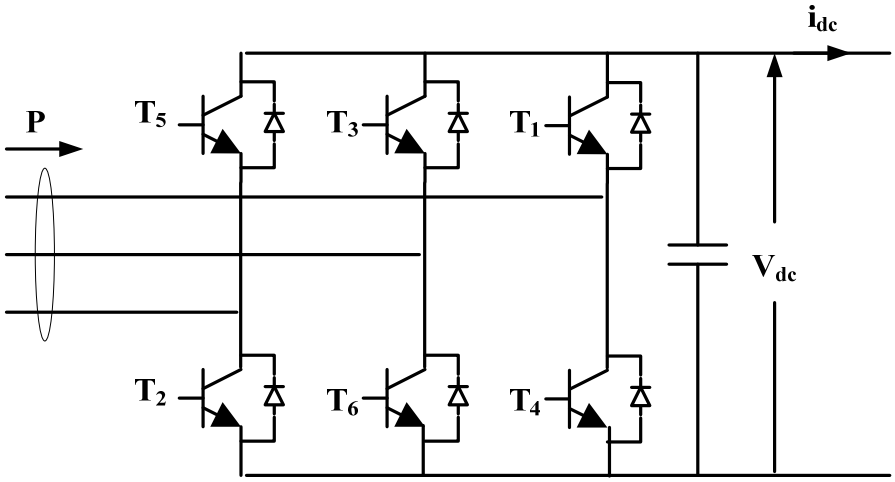

Fig. 4. 10. The rectifier model

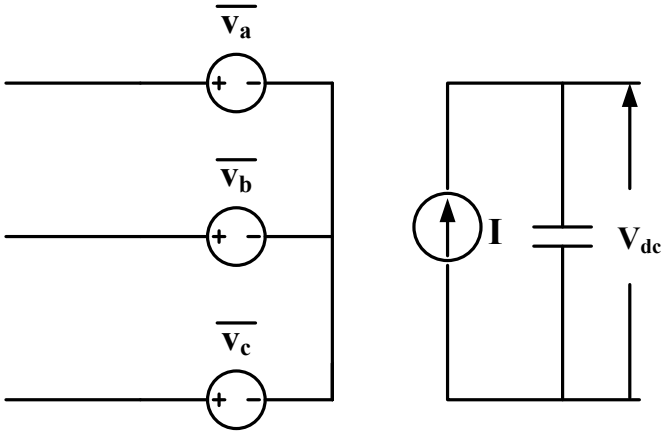

Fig. 4. 11. The rectifier average-value model

The approach used here to obtain voltage and current sources signal values in the rectifier average-value model is illustrated in Fig. 4.12. The rectifier is represented by a block, which inputs $\overline{v_{dc}}$ and P, and outputs $\overline{i_{dc}}$, $\overline{v_d^{rec}}$ and $\overline{v_q^{rec}}$. $\overline{i_{dc}}$ is calculated using $\overline{v_{dc}}$ and P according to (4.12), while $\overline{v_d^{rec}}$ and $\overline{v_q^{rec}}$ are calculated using $\overline{v_{dc}}$.

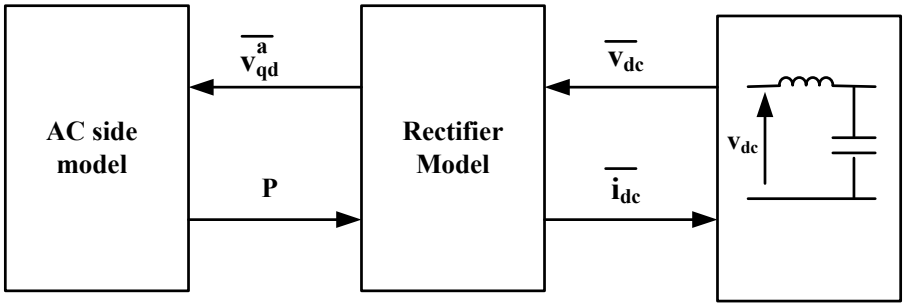

Fig. 4.12. Average-value modeling with rectifier as an algebraic block (Adopted from [26])

Neglecting the relatively small power loss in the rectifier, $\overline{i_{dc}}$ can be calculated using $\overline{v_{dc}}$ and P:

$$\overline{i_{dc}} = \frac{P}{\overline{v_{dc}}} \tag{4.12}$$

According to equations (4.5) and (4.8) and considering the *dq* reference frame is chosen in a way that d-component of voltage is zero, $\overline{v_d^{rec}}$ and $\overline{v_q^{rec}}$ can be calculated as follows:

$$\overline{v_q^{rec}} = \frac{v_{dc} m}{2} \tag{4.13}$$

$$\overline{v_d^{rec}} = 0 \tag{4.14}$$

The corresponding simulation model in PSCAD/EMTDC is illustrated below. The rectifier model has been replaced with dependant voltage and current sources:

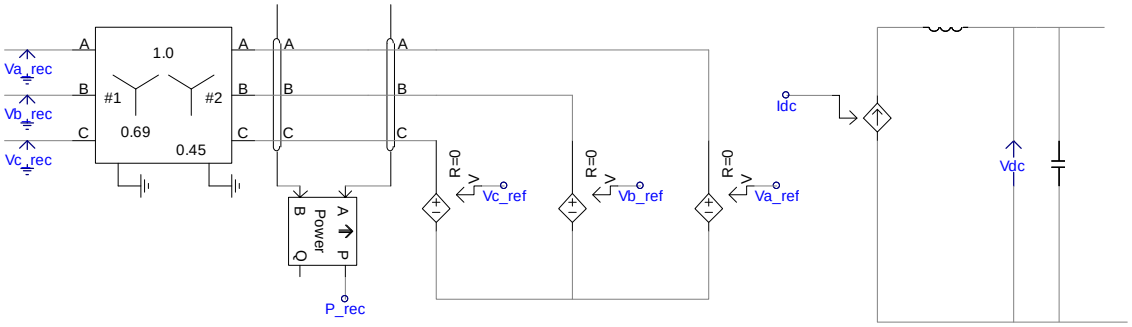

Fig. 4.13. Equivalent average-value model for the rectifier in PSCAD/EMTDC

There are no actual switches in the average-value model. Therefore, the simulation time step can be increased, which results in decreasing the simulation execution time. The results obtained from the detailed model and the dynamic average-value model simulation of the DFIG wind energy conversion system with specifications stated in Table 3.1 along with the corresponding reference values are illustrated in Fig. 4. 14. The simulation time step for the EMT detailed model is 5 µs and for the average-value model is 25 µs.

To compare the simulations speed of the average-value model and the EMT detailed model, the simulation actual execution times for the same simulation run time (10 seconds) are included in the table below. The average-value model reduces the simulation execution time by 65%.

	Actual execution time(s)
Detailed Model	704
Average-value Model	249

Table 4.2. Simulation execution time for average-value model and EMT detailed model

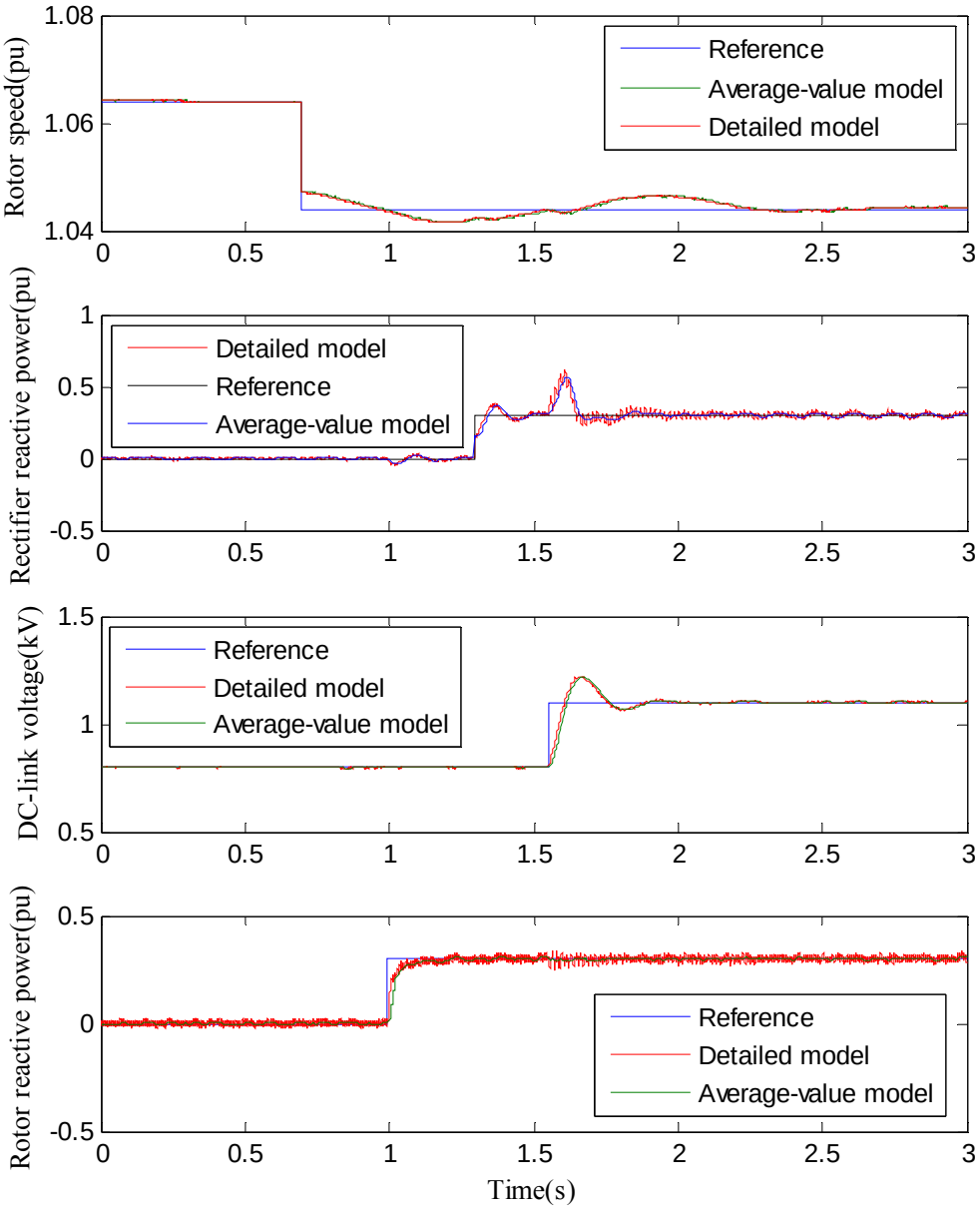

Fig. 4. 14. EMT detailed SPWM and average-value models results

4.3 Reduced Intensity Simulation of a Wind Farm Connected to the Power System Network

Previously, the EMT detailed models (OPWM/SPWM) and their corresponding reduced intensity models of a DFIG wind energy conversion system were described and simulated. In this section, the proposed models are used to simulate a wind farm connected to a test power system. The wind farm is assumed to consist of twenty identical DFIGs connected to the same bus of the power system through a transformer. The test power system is used as an example of a small but representative power system network consisting of generation and loading areas.

In this section, all of the DFIGs are first simulated using the EMT detailed model with SPWM and OPWM techniques separately. Then the reduced intensity simulation techniques are applied, and the simulation execution times are recorded and compared.

The test system includes twelve busses and can be simply divided into three main areas. Area 1 is a generation area with hydro power generators. Area 3 is mainly a load area but with some thermal power generation. Area 2 is located in between Areas 1 and 3, and has some load and some generation which is not sufficient for the loads in this area. A single line diagram of the small test system is illustrated in Fig. 4. 15.

The wind farm simulated in this section is located in Area 2, and consists of twenty identical DFIGs. Each DFIG has the same ratings as those DFIG described in Chapter 3. The DFIGs are connected to Bus 12 via a 0.69 kV/ 22 kV step-up transformer.

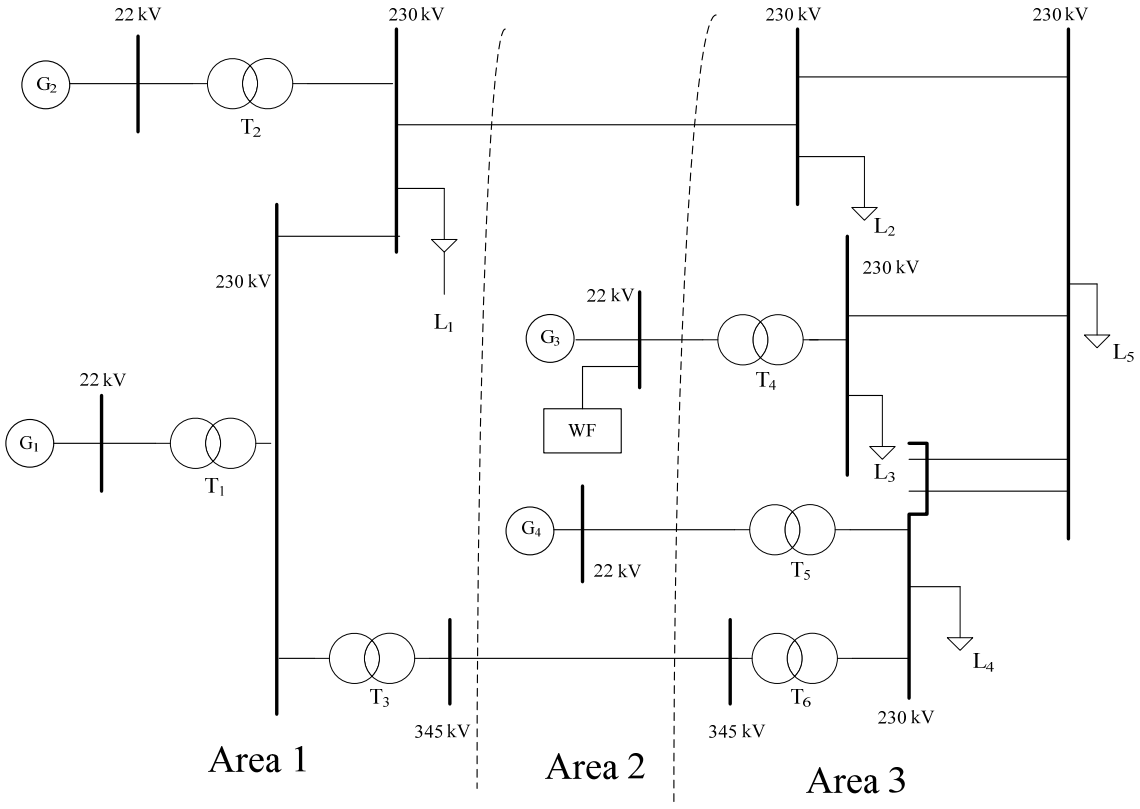

Fig. 4. 15. Wind farm (WF) connected to the 12 bus system

Some technical data of the test system used in the simulations described in this thesis is provided in Table 4.3.

Bus	Nominal Voltage (kV)	Generation (MW)	Load (MVA)
1	230		
2	230		280+j200
3	230		320+j240
4	230		320+j240
5	230		100+j60
6	230		440+j300
7	345		
8	345		
9	22		
10	22	500	
11	22	200	
12	22	300	

Table 4.3. Data of the test power system

Previously five simulation cases in PSCAD/EMTDC were obtained for simulation of a DFIG wind energy conversion system which are summarized below

- EMT detailed model with SPWM scheme
- Switching-function model with SPWM scheme
- Average value model
- EMT detailed model with OPWM scheme
- Switching-function model with OPWM scheme

The system illustrated in Fig. 4. 15. is simulated in PSCAD/EMTDC in five separate cases using the models for simulating a single DFIG as summarized above. The purpose of the wind farm simulation is mainly to compare simulation execution time for different

modeling techniques in the test power system with a wind farm, which contains a number of individual DFIGs.

The simulation execution times for the five cases for the same simulation run time (10 seconds) are summarized below.

	Actual execution time(s)
EMT Detailed OPWM Model	25712
Switching- function OPWM model	22659
EMT Detailed SPWM Model	37206
Switching- function SPWM model	29276
Average-value Model	27704

Table 4.4. Simulation execution time for the wind farm connected to the test power system

In OPWM simulation model, the switching-function modeling technique reduces the simulation execution time by 11%. With SPWM scheme, the switching-function modeling technique and the average-value modeling technique result in reduction of the simulation execution time by 21% and 25%, respectively.

The percentage of reduction in the simulation execution time with the reduced intensity modeling techniques is smaller compared to the case of one DFIG simulation. This is due to the complexity of the test power system used. This test power system has many details which reduce the simulation execution time significantly and the DFIGs are only a part of the complexity.

Normally one would expect that the average model should take the least amount of time for simulation. This however is not seen in Table 4.4. The reason is that the

simulation model of the average-value model includes 19 turbines with the average model and one turbine with the fully-detailed SPWM EMT model. This model is far more demanding than the switching function OPWM and hence the longer simulation time.

Chapter 5

Conclusions, Contributions, and Suggestions for Future Work

The conclusions and contributions of this research are included in section 5.1. Some suggestions for the future work are presented in section 5.2

5.1 Conclusions and Contributions

The conclusions and contributions of this research are summarized as follows.

1. Different types of wind energy conversion systems and their corresponding advantages and disadvantages were briefly discussed. Among the four most commonly used types of wind energy conversion systems, doubly-fed induction generator wind energy conversion system is the main focus of this research.
2. The aerodynamical, mechanical, and electrical aspects of DFIG wind conversion systems were discussed in detail. Also, different configurations of the ac/ac power electronic converters under pulse width modulation schemes were discussed. Back-to-back PWM converter, which is the most conventional ac/ac power electronic converter used in DFIG wind conversion systems, is the focus of this research.
3. The DFIG wind energy conversion system under SPWM and OPWM schemes including the wind turbine, the generator, the power electronic converter and their corresponding control schemes were simulated in detail in PSCAD/EMTDC. This EMT detailed model provided a strong tool for DFIG wind energy conversion system studies with high accuracy, and was used as a benchmark to determine the accuracy and time efficiency of the reduced intensity models.
4. The detailed EMT model is time consuming since at every switching instant the system topology changes and the system admittance matrix should be calculated again. To overcome this issue, two reduced intensity models, switching- function modeling and dynamic average-value modeling were examined, in which the system topology remains the same. These models were used for PSCAD/EMTDC simulation. Case studies show that reasonably accurate results as compared to

those obtained using the EMT detailed simulation model but the simulation execution time is reduced.

5. As the final step, the EMT detailed model and the reduced intensity models were used to simulate the DFIG wind energy conversion systems in a wind farm. The wind farm was connected to a test power system. The two reduced intensity models were applied to the model. Considering the presence of several power electronic switches in a wind farm model which slows the simulation, the reduced intensity models decreased the simulation execution time.
6. In the simulation of a wind farm the reduced intensity models provided some saving in the simulation execution time. In the simulation of one DFIG wind energy conversion system, the reduced intensity models provided higher percentage of reduction in the simulation execution time than in a wind farm simulation.

5.2 Suggestions for Future Work

Some suggestions for future work are given as follows.

1. The set of controlled variables of the back-to-back PWM converter in this research is the rotor speed and the DFIG reactive power for the inverter side of the back-to-back PWM converter, and dc link voltage and rotor reactive power for the rectifier side of it. Although this set of variables is commonly used in DFIG wind energy generation systems, other sets of variables including active power of

the DFIG may be used [30]. It is suggested to implement the detailed, switching-function and average-values models using other control variables to investigate the corresponding reduction in simulation execution time for those models, as they may be useful in some utilities.

2. The focus of this research is on DFIG wind energy conversion systems as they are becoming the most popular setting in wind farms. The proposed models in this thesis can be applied on other wind energy conversion systems using a different type of power electronic converter and/or a different type of generator.
3. In this research, the simulation models were developed in PSCAD/EMTDC, which is a well-established and commenly used software for electromagnetic transients simulation. However, the simulation execution time may vary for different software packages. The same models can be simulated in another suitable program such as MATLAB SIMULINK to record the simulation execution times and the corresponding execution time reduction for each reduced intensity model.

References

[1] M. Sathyajith, G. S. Philip, *Advances in Wind Energy Technology,* Springer, 2011.

[2] L. Surugiu, I. Paraschivoiu, "Environmental, Social and Economic Aspects of Wind Energy", *Energy Conversion Engineering Conference and Exhibit* (IECE), USA, pp. 1167-1174, 2000.

[3] World Wind Energy Report 2010, World Wind Energy Association (WWEA), April 2011, Available at www.wwindea.org

[4] Canadian Wind Energy Association (CanWEA), Spring 2011, Available at www.canwea.ca

[5] H. Kowalski and J. Mathur, *Introduction to wind Energy Systems*, Springer, 2009.

[6] M. Stiebler, *Wind Energy Systems for Electric Power Generation*, Springer, 2008.

[7] H. Li, Z. Chen, "Overview of different wind generator systems and their comparisons," *IET Renew. Power Gener*, Vol. 2, pp. 123–138, 2008.

[8] Wei Qiao, "Dynamic Modeling of Wind Farms with Fixed-Speed Wind Turbine Generators," *In Proc. Of the 2007 IEEE Power Engineering Society General Meeting*, USA.

[9] H. Sun, Y. Ren, H. Li, Z. An, J. Liu, H. Hu, H. Liu," DFIG Wind Power Generation Based on Back-to-back PWM Converter*," Proceedings of the 2009 IEEE International Conference on Mechatronics and Automation*, China, pp. 2276 – 2280.

[10] W. W. Price, J. J. Sanchez-Gasca, ”Simplified wind turbine generator aerodynamic models for transient stability analysis,” *In Proc. of the 2006 IEEE Power Systems Conference and Exposition.*

[11] Dragan Maksimovic, Aleksandar M. Stankovic, V. Joseph Thottuvelil, George C. Verghese, ”Modeling and Simulation of Power Electronic Converters,” Proceedings of the IEEE, Vol. 89, No. 6, pp 898-912, June 2001.

[12] L. Mihet-Popa, F. Blaabjerg, and I. Boldea, “Wind turbine generator modeling and simulation where rotational speed is the controlled variable,” *IEEE Trans. Ind. Appl.*, Vol. 40, No. 1, pp. 3 – 10, 2004.

[13] Abram Perdana, “Dynamic Models of Wind Turbines,” Ph.D. dissertation, Energy and Environment Dept., Chalmers University of Technology, Sweden, 2008.

[14] J. G. Slootweg, H. Polinder, and W. L. Kling, “Dynamic modeling of a wind turbine with doubly fed induction generator,” *In Proc. IEEE Power Eng. Soc. Summer Meeting,* Vancouver, Canada, July 2001.

[15] D. Hansen, C. Jauch, P. Sørensen, F. Iov, F. Blaabjerg, "Dynamic wind turbine models in power system simulation tool DIGSILENT," Annual Report, Danmarks Tekniske Universitet, Risø Nationallaboratoriet for Bæredygtig Energi, Roskilde, 2007.

[16] J. G. Slootweg, H. Polinder*,* W. L. Kling*,* “Representing Wind Turbine Electrical Generating Systems in Fundamental Frequency Simulations,” *IEEE Transaction on Energy Conversion*, Vol. 18, No. 4, pp 516 – 524, December 2003.

[17] Wei Qiao, Wei Zhou, José M. Aller, Ronald G. Harley*,”* Wind Speed Estimation Based Sensorless Output Maximization Control for a Wind Turbine Driving a DFIG,” *IEEE Trans. On Power Electronics*, Vol. 23, No. 3, pp 1156 – 1169, May 2008.

[18] Slavomir Seman, “Transient performance analysis of wind-power induction generators,” Ph.D. dissertation, Department of Electrical and Communications Engineering, Helsinki University of Technology, 2006.

[19] S. Masoud Barakati, “Modeling and Controller Design of a Wind Energy Conversion System Including a Matrix Converter,” Ph.D. dissertation, Electrical and Computer Engineering, University of Waterloo, 2008.

[20] M. H. Rashid, *Power Electronics: Circuits, Devices, and Applications*, Prentice-Hall India, 2003.

[21] S. Filizadeh, *Advanced Power Electronic* course notes, Dept. of Electrical and Computer Engineering, University of Manitoba, 2010.

[22] A. Mehrizi, “Advanced Modulation Techniques for Power Converters,” M.Sc. dissertation, Dept. of Electrical and Computer Engineering, University of Manitoba, 2011.

[23] R. Pena, J.C. Clare, G.M.Asher, “A doubly fed induction generator using back-to-back PWM converters supplying an isolated load from a variable speed wind turbine,” *IEE Proc.-Electr. Power Appl.,* Vol. 143. No. 5, September 1996.

[24] R. Pena, J.C. Clare, G.M.Asher, “Doubly fed induction generator using back-to-back PWM converters and its application to variable-speed wind-energy generation,” *IEE Puoc.-Electr. Power Appl.*, Vol. 143, No 3, May 1996.

[25] Yazhou Lei, Alan Mullane, Gordon Lightbody, and Robert Yacamini,”Modeling of the Wind Turbine with a Doubly Fed Induction Generator for Grid Integration Studies,” *IEEE Trans. On Energy Conversion*, Vol. 21, No. 1, MARCH 2006.

[26] Juri Jatskevich, Steven D. Pekarek, Ali Davoudi, , "Parametric Average-Value Model of Synchronous Machine-Rectifier Systems," *IEEE Trans. on Energy Conversion*, Vol. 21, No. 1, March 2006.

[27] S. Chiniforoosh, J. Jatskevich, A. Yazdani, V. Sood, V. Dinavahi, J. A. Martinez, and A. Ramirez," Definitions and Applications of Dynamic Average Models for Analysis of Power Systems," IEEE Trans on Power Delivery, Vol. 25, No. 4, October 2010.

[28] D. Maksimovic," Synthesis of PWM and Quasi resonance dc-dc converters," Ph.D. dissertation, California Institute of Technology, Jan. 1989.

[29] S. Jiang, U.D. Annakkage, A.M.Gole, "A Platform for Validation of FACTS Models," *IEEE Trans. On Power Delivery*, Vol. 21, No. 1, Jan. 2006.

[30] A. Tapia, G. Tapia, J. X. Ostolaza, J.R. Saenz, "Modeling and Control of a wind turbine driven doubly fed induction generator," *IEEE Trans on Energy Conversion*, Vol. 18, No. 2, June 2003.

[31] Paul C. Krause, Oleg Wasynczuk, Scott D. Sudhoff, *Analysis of Electric Machinery*, IEEE Press, 1995